國 立 交 通 大 學

電子工程學系 電子研究所碩士班

碩 士 論 文

運用功率延遲輪廓近似之線性最小均方差通道估計於 LTE 下行時變通道傳輸

LMMSE Channel Estimation with Power-Delay Profile Approximation for LTE Downlink Transmission over Time-Variant Channels

研 究 生 ： 楊葆崧

指 導 教 授 ： 林大衛 教授

中 華 民 國 一 ○ 二 年 八 月

運用功率延遲輪廓近似之線性最小均方差通道估計於 LTE 下行時變通道傳輸

LMMSE Channel Estimation with Power-Delay Profile Approximation for LTE Downlink Transmission over Time-Variant Channels

研 究 生：楊葆崧　　　　Student: Bao-Song Yang

指導教授：林大衛　　　　Advisor: Dr. David W. Lin

國 立 交 通 大 學

電子工程學系　　電子研究所碩士班

碩 士 論 文

A Thesis
Submitted to Department of Electronics Engineering & Institute of Electronics
College of Electrical and Computer Engineering
National Chiao Tung University
in Partial Fulfillment of the Requirements
for the Degree of Master of Science
in
Electronics Engineering
August 2013
Hsinchu, Taiwan, Republic of China

中 華 民 國 一 ○ 二 年 八 月

運用功率延遲輪廓近似之線性最小均方差通道估計於 LTE 下行時變通道傳輸

研究生：楊葆崧　　　　　　　　指導教授：林大衛 博士

國立交通大學

電子工程學系　電子研究所碩士班

摘要

正交分頻多重進接(OFDMA)技術近年來在行動環境中廣受注目，而且已經應用在許多數位通訊應用中。採用 OFDMA 一個最主要的原因是其抗頻率選擇性衰變的能力。在此篇論文中，我們聚焦於 LTE 與 LTE-A OFDMA 下行通道估測部分。

本篇論文最主要採用的通道估測方法為線性最小均方差(LMMSE)通道估測法。在使用 LMMSE 通道估測法於多載波傳輸系統中，我們需要知道通道相關性函數。 這在參考訊號(RS)較少的傳輸系統中帶來了問題。為了解決這個問題，我們將通道的功率延遲輪廓做近似，使其可以完全被兩個通道延遲參數所定義，這兩個參數為初始延遲參數以及方均根延遲擴展參數。除此之外，我們發展了一個技術來估測這些參數。為了增進估測參數的準確度，我們引入了虛參考響應生成的概念來達成我們的目標。接著我們可以找到功率延輪廓遲近似所相對應的自相關矩陣。最後藉由這個自相關矩陣，使用 LMMSE 通道估測法來估計次載波上的資訊。我們藉由加成性白高斯雜訊通道來驗證我們的模擬程式以及通道估測方法，接著在幾個多路徑通道做模擬。

在本篇論文中，我們首先簡介 LTE 與 LTE-A 下行的標準機制。接著，我們依造兩種標準機制分別各傳輸情形下介紹所用的通道估測方法並探討其估測效能。

LMMSE Channel Estimation with Power-Delay Profile Approximation for LTE Downlink Transmission over Time-Variant Channels

Student: Bao-Song Yang   Advisor: Dr. David W. Lin

Department of Electronics Engineering

Institute of Electronics

National Chiao Tung University

Abstract

Orthogonal frequency division multiple access (OFDMA) technique has drawn much interest recently in the mobile transmission environment and been successfully applied to a wide variety of digital communications applications over the past several years. One of the main reason to use OFDMA is its robustness against frequency selective fading. We focus on the OFDMA downlink (DL) channel estimation based on LTE and LTE-A.

The main channel estimation method is linear-minimum-mean-square-error (LMMSE) channel estimation in this thesis. In LMMSE channel estimation for multicarrier systems, one needs to know the channel correlation function. This brings up a problem for systems with a small number of reference signals (RSs). To solve this problem, we approximate the channel power-delay profile (PDP) that can completely be described in two channel delay parameters, i.e., the initial delay and the root-mean-square (RMS) delay. In addition, we develop a technique to estimate these delay parameters. For improving the accuracy of the estimated channel delay

parameters, we employ an idea, producing pseudo RR, to meet our purpose. Then we find the autocorrelation function associated with the approximate PDP. Finally base on this autocorrelation function, do LMMSE filtering to estimate the data subcarrier response. We verify our simulation program and channel estimation methods on AWGN channel and then do the simulation on several multipath channels.

In this thesis, we first introduce the standard of the LTE and LTE-A DL. Then we describe the channel estimation methods we use and discuss the performance in each transmission condition for LTE and LTE-A.

誌 謝

　　於 2013 八月末，這本論文終於要完成了，在這一路上我受到了許多人的幫助。其中最感謝的，莫過於指導教授林大衛老師，在這兩年多的相處中，老師總是一路耐心的引領著我們，對於我們遇到的問題，總是能夠給予我們適切的方向。平時對於我們也是相當的關心，答應我們的承諾，也總是盡心盡力的去完成，特別是在論文來回修改的時期，平常總是中氣十足的老師，為了趕著將修改好的論文交給我們，竟然難得出現了黑眼圈！對於老師的感激之情，學生葆崧難以用筆墨來形容。

　　另外，在這裡也要好好感謝 CommLab 的各位夥伴。林 Group 的各位兄弟：(怪盜基)男鑫、夏銘和信宏，真的很感謝一路上的互相扶持，不論是在修課、做研究以及找工作，我們都毫無保留，認真的給予彼此建議，讓我們都能夠順利的成長，很慶信自己能夠跟你們做夥伴。還有杭 Group、簡 Group 以及桑 Group，一路上有你們的陪伴，不論在研究或者休閒上都讓我常常擁有不同的感受，在這邊小弟祝各位夥伴們皆能早日結交男/女朋友。而已經離開學校的學長們，感謝你們在我遇到各種問題時所給的種種建議，沒有你們的經驗分享，對於研究以及找工作都還不太熟悉的我可能都還要摸索好一陣子，謝謝你們對我的照顧。

　　最後要感謝我的家人、朋友以及陪伴著我八年的宜涵；在研究的路上，在我遇到各種挫折而心情苦悶的時候，心情及口氣有時會不太和善，然而你們總是能夠給予我鼓勵以及陪伴，讓我的內心總是能夠充滿著正面的能量，這邊我真的是由衷地感謝各位的包容以及陪伴。
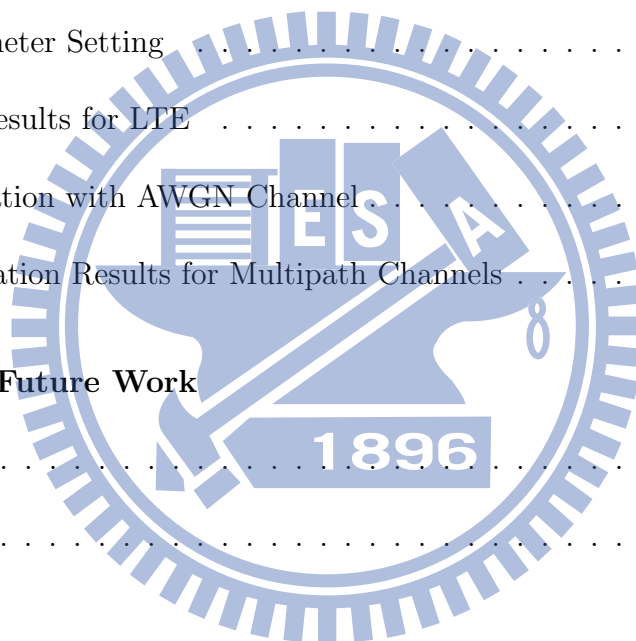
<div align="right">楊葆崧</div>

<div align="right">民國一〇二年八月 於新竹</div>

Contents

List of Figures

List of Tables

Chapter 1

Introduction

Orthogonal frequency division multiple access (OFDMA) is the chosen multiple access scheme for the downlink in the 3rd Generation Partnership Project (3GPP) Long Term Evolution (LTE) and LTE-Advanced (LTE-A) cellular mobile communication standards [7]. The LTE-A standard is a standard designed to increase the capacity and speed of mobile telephone networks and be obedient to IMT-Advanced requirements. It is backwards compatible with LTE and uses the same frequency bands, while LTE is not backwards compatible with 3G systems. LTE is introduced in 3GPP release 8 whereas LTE-A, release 10. Much of 3GPP release 8 focuses on adopting expected 4G mobile communication technologies, including an all-IP flat networking architecture. The 3GPP is keeping working on evolution the LTE set of standards towards future releases.

Our study focuses on LTE and LTE-A physical downlink shared channel (PDSCH) estimation schemes based on the 3GPP TS 36.211 release 8 [5] and release 10 [6]. In particular, we consider the linear minimum mean-square error (LMMSE) approach proposed in [2].

Reference signal (RS) aided channel estimation is widely employed in today's coherent wireless orthogonal frequency-division multiplexing (OFDM) systems. The subcarriers that carry RSs are usually dispersed in frequency and in time. The LMMSE technique is also

1

known as Wiener filtering. Given some initial channel estimates at RS subcarriers, the LMMSE channel estimate at any subcarrier, is given by [1]

$$\hat{H}_{RS,LMMSE} = R_{H_{RS}H_{RS,P}}(R_{H_{RS,P}H_{RS,P}} + \frac{\beta}{SNR}I)^{-1}\hat{H}_{RS,P}, \tag{1.1}$$

where $\hat{H}_{RS,P}$ is the initial channel estimation vector at the RS subcariers, $R_{H_{RS,P}H_{RS,P}}$ is the autocorrelation matrix of the channel responses at the RS subcarriers, $R_{H_{RS}H_{RS,P}}$ is the crosscorrelation matrix of the channel responses at the RS subccaries and that to be estimated, β is a constant depending on the type of modulation, SNR is the average signal-to-noise ratio, I is the identity matrix with same size as $R_{H_{RS,P}H_{RS,P}}$ and the subscript $(\cdot)^H$ denotes Hermitian transpose. We note that a convenient and frequently used method to estimate $\hat{H}_{RS,P}$ is the least-squares (LS) method, which merely divides the received signal at each RS subcarrier by the known pilot value there to obtain the estimated response there [1].

To carry out the LMMSE estimation, one needs to know $R_{H_{RS,P}H_{RS,P}}$, $R_{H_{RS}H_{RS,P}}$, and SNR. The estimation of SNR can be achieved by measuring the received power at the null subcarriers. The estimation of $R_{H_{RS,P}H_{RS,P}}$ and $R_{H_{RS}H_{RS,P}}$, however, presents a problem. One aspect of the problem has to do with the fact that an accurate estimate requires averaging over sufficiently samples. But when the channel is time-varying, one may not have this luxury within the coherence time. Another aspect of the problem is about $R_{H_{RS}H_{RS,P}}$. The estimation of $R_{H_{RS}H_{RS,P}}$ requires interpolation. How to get crosscorrelation from autocorrelation is a problem.

To overcome the above problems, one approach is to employ a simple model for the channel power-delay profile (PDP). A common choice is the exponentially decaying PDP, which is especially suitable for the in-door environment [4]. For it, the entire second-order channel statistics are defined by the mean delay τ_μ and the root-mean-square (RMS) delay spread τ_{rms}. Given τ_μ and τ_{rms}, one can calculate $R_{H_{RS,P}H_{RS,P}}$ and $R_{H_{RS}H_{RS,P}}$. The price

paid for this PDP model is that the true PDP may not be an exponential one, and the modeling error may lead to performance degradation. But [2] shows that exponential PDP based LMMSE channel estimation can yield good performance and is amenable to typical RS-transmitting OFDM signal structures. Therefore, the present study will consider the exponential PDP. The remaining chaoters of this thesis is organized as follows.

- In chapter 2, we introduce some OFDMA basics in the LTE and LTE-A downlink standards.

- In chapter 3, we describe the considered downlink transmission system structure and present some channel estimation techniques.

- In chapter 4, we present some simulation results and discuss the performance of differ- ence channel estimation methods.

- In chapter 5, we give the conclusion and indicate some items of potential future work.

1.1 Contributions

In this thesis, we have two techniques to estimate channel delay parameters. One is the technique of [2] for downlink channel estimation in LTE and LTE-A, another is derived by ourselves. Thus we can do LMMSE filtering without knowing the correlation matrix of the channel responses previously. That is to say, we can do LMMSE filtering everywhere. The time-variant issue is also considered. We can achieve the requirement specified in LTE and LTE-A, namely, we can support the case when vehicular is travelling at a speed of 350 km/h. Furthermore, we also employ several methods for generating pseudo reference response (RR), with which we will get further improved especially in highly frequency selective environments. In some case, the performance with pseudo RR is over ten times better than the performance without pseudo RSs.

Chapter 2

Overview of LTE and LTE-A Downlink Specifications

The contents are mainly taken from [5, 6, 7, 10].

The goal of LTE is to provide a high-data-rate, low-latency and packet-optimized radio access technology supporting flexible bandwidth configurations [5, 7]. In addition, new network architecture is designed with the target to support packet-switched traffic with seamless mobility, quality of service and minimal latency.

The air-interface related features of the LTE system are summarized in Table 2.1. The system supports flexible bandwidths thanks to orthogonal frequency-division multiple access (OFDMA) and single-carrier frequency division multiple access (SC-FDMA) schemes. In addition to frequency division duplexing (FDD) and time division duplexing (TDD), half-duplex FDD is allowed to support low cost user equipment (UE). Unlike FDD, in half-duplex FDD operation a UE is not required to transmit and receive at the same time. This avoids the need for a costly duplexer in the UE.

The system is initially optimized for low speeds up to 15 km/h. However, the LTE system is also required to support speeds from 15 to 120 km/h with high performance and in excess of 350 km/h with some performance degradation.

Table 2.1: LTE System Attributes [7, Table 1.1]

Bandwidth	1.4–20 MHz	
Duplexing	FDD, TDD, half-duplex FDD	
Mobility	350 km/h	
Multiple access	Downlink	OFDMA
	Uplink	SC-FDMA
multi-input multi-output (MIMO) modes	Downlink	$2 \times 2, 4 \times 2, 4 \times 4$
	Uplink	$1 \times 2, 1 \times 4$
MIMO data rates	Downlink	173 and 326 Mb/s for 2×2 and 4×4 MIMO, respectively
	Uplink	86 Mb/s with 1×2 antenna configuration
Modulation	QPSK, 16-QAM and 64-QAM	
Channel coding	Turbo code	
Other techniques	Channel sensitive scheduling, link adaptation, power control, inter-cell interference coordination (ICIC) and hybrid ARQ	

For LTE, the downlink (DL) has a maximum of four layers multi-input multi-output (MIMO) transmission, while the uplink has a maximum of one for one UE. It can support 4×4 MIMO in the DL. In the uplink, there is no MIMO capability from a single UE. LTE-A can support up to eight streams in the DL with eight receivers in the UE, giving a possibility of 8×8 MIMO in the DL. And in the UL, the UE is allowed to support up to four transmitters, thereby offering a possibility of up to 4×4 transmissions.

In this chapter, we introduce some basic concepts of OFDM, OFDMA and the physical channel structure in LTE [5] and LTE-A specifications [6], the letter focusing on the DL part especially.

2.1 Overview of OFDM and OFDMA

The contents of this section are mainly taken from [7, Chepter 3].
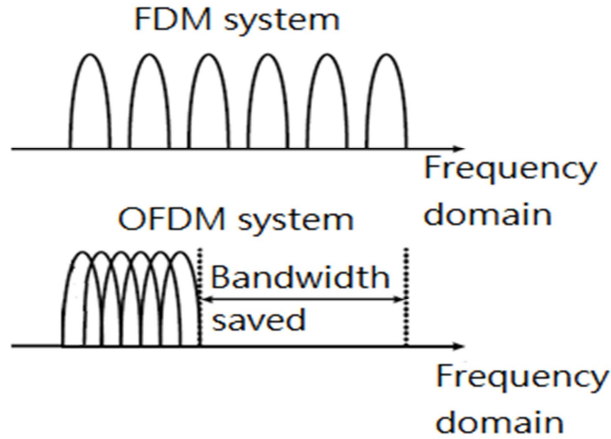
Figure 2.1: Traditional FDM system versus OFDM system.

2.1.1 OFDM

Orthogonal frequency division multiplexing (OFDM) was first proposed almost five decades ago by R. W. Chang [8]. The scheme was soon analyzed by Saltzberg [9]. The name OFDM comes from the fact that the frequency response of the subchannels are overlapping but orthogonal; its spectrum efficiency is better than traditional FDM, as depicted in Figure 2.1.

Data are transmitted by parallel channels in OFDM system, so serial data should be transformed into converted data first. After we get parallel data, N-point inverse fast Fourier transform (IFFT) is taken, so as to generate samples which are sum of N orthogonal subcarrier signals. These subcarriers can be defined

$$\Phi_k(t) = e^{j2\pi f_k t} = e^{j2\pi k \Delta f t} = e^{j\frac{2\pi kt}{T_{sym}}}, \ k = 0, 1, ..., N-1, \tag{2.1}$$

where f_k denotes the frequency of the kth subcarrier, Δf denotes subcarrier spacing and T_{sym} denotes OFDM symbol duration. These subcarriers are orthogonal because the integral of their pairwise products over a symbol period is zero, that is,

$$\int_0^{T_{sym}} \Phi_k(t)\Phi_i^*(t)dt = \int_0^{T_{sym}} e^{j\frac{2\pi kt}{T_{sym}}} e^{-j\frac{2\pi it}{T_{sym}}} dt = \int_0^{T_{sym}} e^{j\frac{2\pi(k-i)t}{T_{sym}}} = \begin{cases} T_{sym}, & \text{if } k = i, \\ 0, & \text{if } k \neq i. \end{cases} \tag{2.2}$$

6
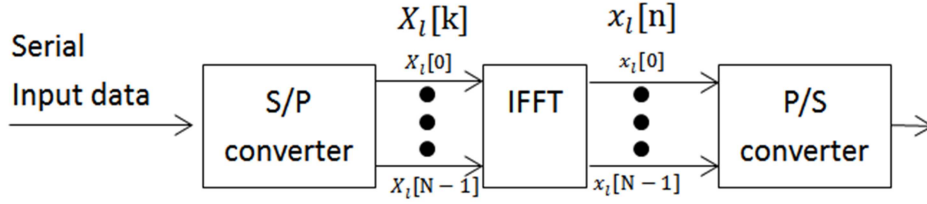
Figure 2.2: A baseband equivalent illustration of modulation in an OFDM system.

The transmitted signal, which are referred to as OFDM symbols, are produced by combining data subcarriers. The transmitted signal is given by

$$x_l(t) = \sum_{l=0}^{\infty} \sum_{k=0}^{N-1} X_l(k) \Phi_k(t) = \sum_{l=0}^{\infty} \sum_{k=0}^{N-1} X_l(k) e^{j\frac{2\pi kt}{T_{sym}}}, \quad lT_{sym} < t \leqslant (l+1)T_{sym}, \qquad (2.3)$$

where $x_l(t)$ denotes the lth transmit symbol at time t and $X_l(k)$ denotes the lth transmit symbol at the kth subcarrier. The continuous-time baseband OFDM signal in (2.3) can be sampled at $t = lT_{sym} + nT_s$ with $T_s = T_{sym}/N$ to yield the correponding discrete-time OFDM symbol as

$$x_l[n] = \sum_{k=0}^{N-1} X_l[k] e^{j\frac{2\pi kn}{N}} \text{ for } n = 0, 1, ..., N-1. \qquad (2.4)$$

Note that (2.4) turns out to be the N-point IFFT of data symbols $X_l(k)$, $k = 0, 1, ..., N-1$. The entire process is illustrated in Figure 2.2. For demodulation, by (2.2) we can detect the data on kth subcarrier by integrating the product of the OFDM symbol and the complex conjugate of the kth subcarrier. The discrete-time version is shown in Figure 2.3 and can be expressed as

$$
\begin{aligned}
Y_l[k] &= \sum_{n=0}^{N-1} y_l[n] e^{-j2\pi kn/N} \\
&= \sum_{n=0}^{N-1} \left\{ \frac{1}{N} \sum_{i=0}^{N-1} X_l[i] e^{j2\pi in/N} \right\} e^{-j2\pi kn/N} \\
&= \frac{1}{N} \sum_{n=0}^{N-1} \sum_{i=0}^{N-1} X_l[i] e^{-j2\pi(k-i)n/N} = X_l[k].
\end{aligned}
\qquad (2.5)
$$

7
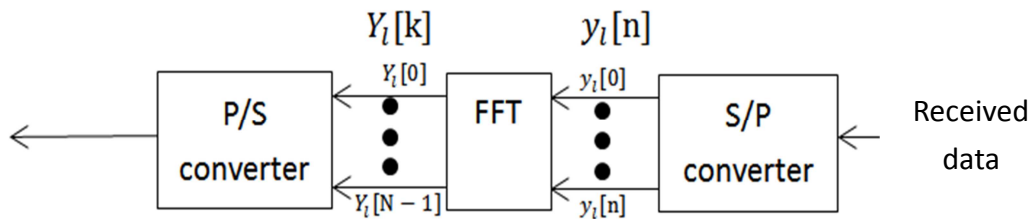
Figure 2.3: A baseband equivalent illustration of demodulation in an OFDM system.

2.1.2 OFDMA

In general, OFDM is a transmission technique in which all subcarriers are used for transmitting the symbols of a single user. Although OFDM is not a multiple access technique by itself, it can be combined with existing multiple access technique such as TDMA (time division multiple access), FDMA (frequency division multiple access), and CDMA (code division multiple access) for a multiuser system. We only treat OFDMA because it is used in LTE and LTE-A.

As depicted in Figure 2.4, the OFDMA system assigns a subset of subcarriers to each user, where the number of subcarriers of a specific user can be adaptively varied in each symbol. As users in the same cell may have different signal-to-noise ratios (SNRs), it would be more efficient to allow the multiple users each uses a subset of subcarriers with a better channel condition, rather than let a single user use all subcarriers at one time. Improvement in the bandwidth efficiency with the former condition is referred to as multiuser diversity gain. OFDMA is a technique that can leverage the multiuser diversity gain inherent to the multicarrier system.

2.1.3 Cyclic Prefix

Cyclic prefix (CP), a copy of the last part of the OFDMA symbol (see Fig. 2.5), is used in OFDM and OFDMA systems to overcome the intersymbol interference (ISI) and inter-
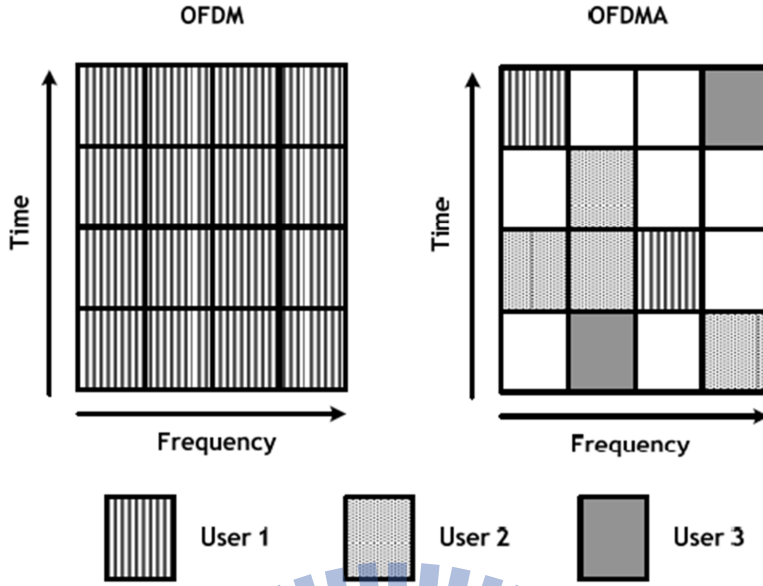
Figure 2.4: OFDMA versus OFDM.

carrier interference (ICI) problems. A copy of the last T_G of the useful symbol period is used to collect multipaths while maintaining the orthogonality of subcarriers. However, the transmitted energy increases with the length of the guard time while the received energy remains the same, because the CP is discarded in the receiver. The multiuser channel is usually assumed to be substantially invariant within one-block (or one-symbol) duration. The channel delay spread plus symbol timing mismatch is usually assumed to be smaller than the CP duration. In this condition, users do not interfere with each other when there is proper time and frequency synchronization. As depicted in Figure 2.6, CP is added before transmission to generate $s_l[n]$. After passing through the channel $h_l[n]$, white Gaussian noise $z_l[n]$ is added. Thus the received signal is given by

$$r_l[n] = \sum_{m=0}^{\infty} h_l[m]s_l[n-m] + z_l[m]. \tag{2.6}$$

After removing CP, the received samples $r_l[n]$ become $y_l[n]$, $n = 0, 1, ..., N-1$, whose FFT is given by

9
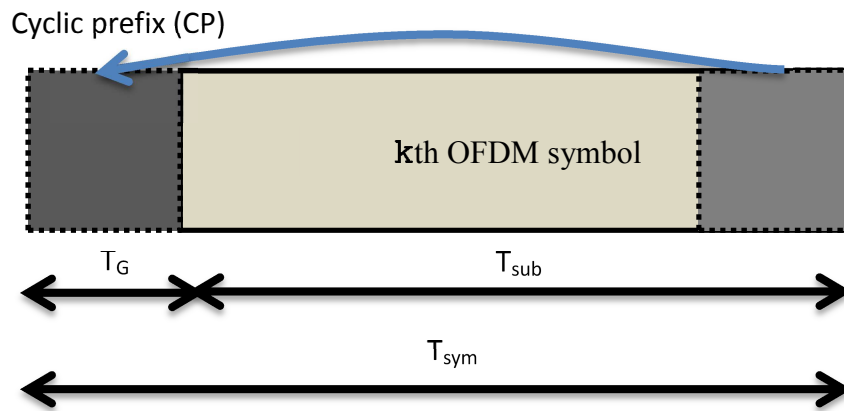
Figure 2.5: OFDM symbols with CP.
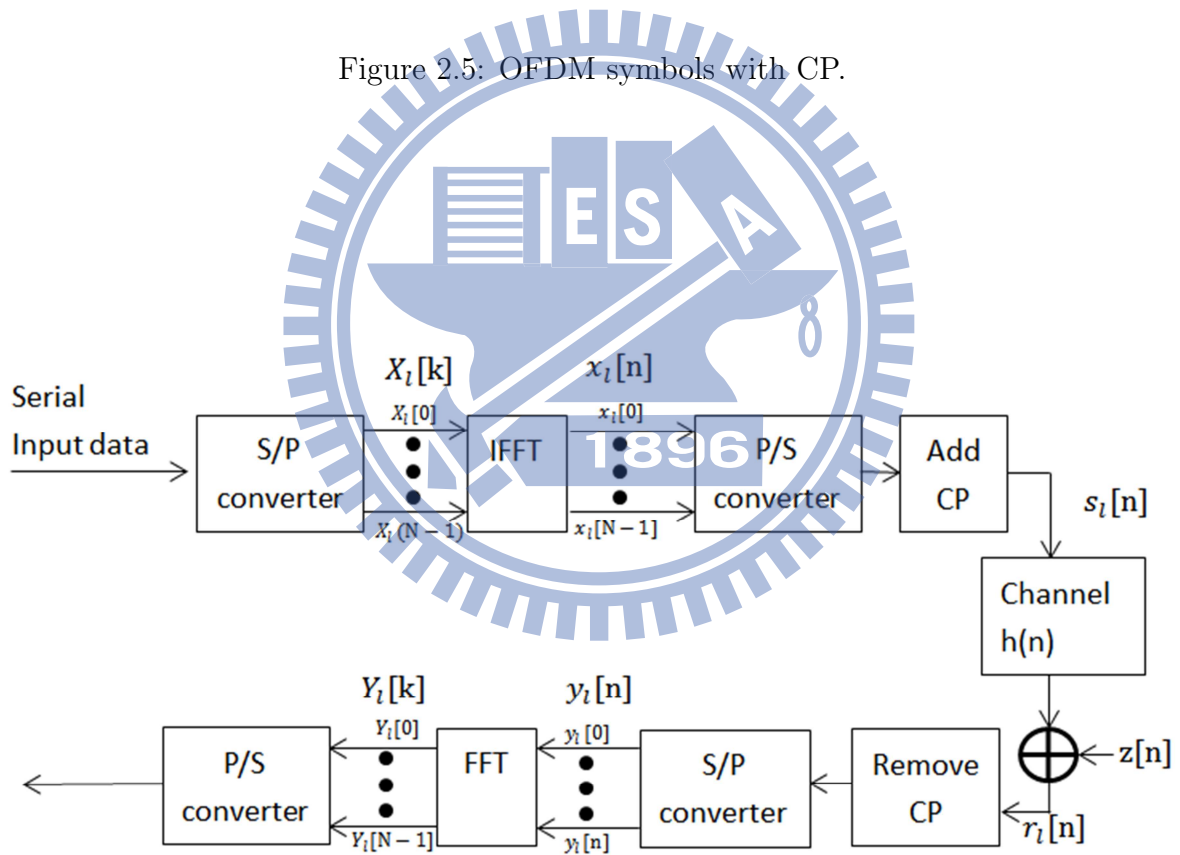
Figure 2.6: OFDM baseband transmission system structure.

10

$$
\begin{aligned}
Y_l[k] &= \sum_{n=0}^{N-1} y_l[n] e^{-j2\pi kn/N} \\
&= \sum_{n=0}^{N-1} \left\{ \sum_{m=0}^{\infty} h_l[m] x_l[n-m] + z_l[n] \right\} e^{-j2\pi kn/N} \\
&= \frac{1}{N} \sum_{i=0}^{N-1} \left\{ \left\{ \sum_{m=0}^{\infty} h_l[m] e^{-j2\pi im/N} \right\} X_l[i] \sum_{n=0}^{\infty} e^{-j2\pi(k-i)n/N} \right\} e^{-j2\pi kn/N} + Z_l[k] \\
&= H_l[k] X_l[k] + Z_l[k],
\end{aligned} \tag{2.7}
$$

where $X_l[k]$, $Y_l[k]$, $H_l[k]$ and $Z_l[k]$ denote the kth subcarrier frequency response of the lth transmitted symbol, received symbol, channel frequency response and noise in the frequency domain, respectively. From the last equality in (2.7), we can find that the OFDM system can be regarded as simply multiplying the input symbol by the channel frequency response in the frequency domain. Since $Y_l[k] = H_l[k] X_l[k]$ in absence of noise, the transmitted symbol at each subcarrier can be recovered by one-tap equalization, which simply divides the received symbol by the channel frequency response to recover the transmitted data, i.e., $\hat{X}_l[k] = Y_l[k]/H_l[k]$ where $\hat{X}_l[k]$ denotes the equalized signal value. Note that $Y_l[k] \neq H_l[k] X_l[k]$ without CP, since $FFT\{y_l[n]\} \neq FFT\{x_l[n]\} \cdot FFT\{h_l[n]\}$ when $y_l[n] = x_l[n] * h_l[n]$, where $*$ denotes convolution. Insertion of CP in the transmitted signal makes it circularly convolved with the channel impulse response, i.e., $y_l[n] = x_l[n] \otimes h_l[n]$, where $\otimes$ denotes circular convolution, which yields $Y_l[k] = H_l[k] X_l[k]$ as desired in the receiver.

2.2 Frame Structure in LTE

The contents of this section are mainly taken from [6].

Throughout the specification for frame structure in LTE, the size of various fields in the time domain (TD) is normally expressed in time units of $T_s = 1/(15000 \times 2048)$ seconds. DL and UL transmissions are organized into radio frames with frame duration that equals $T_f = 307200 \times T_s = 10$ ms. Frame structure type 1, which applies to both full duplex and
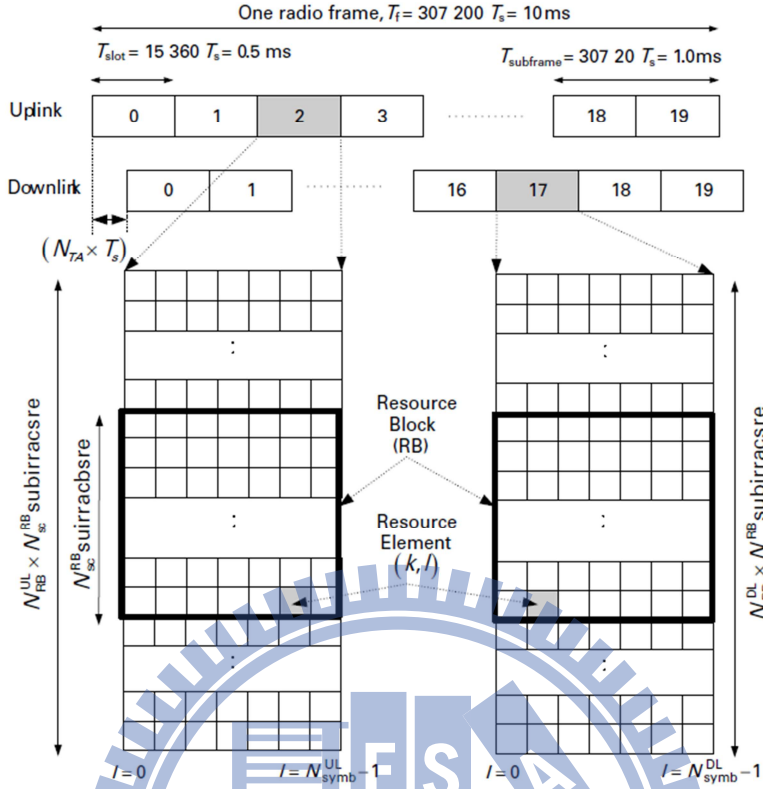
Figure 2.7: Frame structure type 1 [7, Figure 8.2].

half duplex FDD, is shown in Figure 2.7. There are 20 slots in a radio frame with length $T_{slot} = 15360 \times T_s = 0.5$ ms, numbered from 0 to 19. A subframe consists of two consecutive slots where subframe i consists of slots $2i$ and $2i + 1$. For FDD, there are 10 subframes for both DL and UL transmissions in each 10 ms interval, where UL and DL transmissions are separated in the frequency domain. In half-duplex FDD operation, the UE cannot transmit and receive at the same time while there are no such restrictions in full-duplex FDD.

A resource block (RB) is defined as N_{SC}^{RB} consecutive subcarriers in the FD and N_{symb}^{DL} OFDM symbols in the DL or N_{symb}^{UL} SC-FDMA symbols in the UL. An RB therefore consists of $N_{SC}^{RB} \times N_{symb}^{DL}$ resource elements in the DL and $N_{SC}^{RB} \times N_{symb}^{UL}$ resource elements in the UL. This corresponds to 180 kHz of bandwidth in the FD and one slot in the TD. The overall transmission bandwidth parameters and RB parameters are listed in Table 2.2. The number

12

Table 2.2: Bandwidth Parameters and RB Parameters [6, Table 8.1]

Channel bandwidth(MHz)	1.4	3	5.0	10.0	15.0	20.0
Resource block (RB) bandwidth (kHz)	180					
Number of available RBs (N_{RB}^{DL})	6	15	25	50	75	100
Number of subcarriers	72	180	300	600	900	1200

Table 2.3: RB Parameters [6, Table 5.2.3-1]

Configuration		N_{sc}^{RB}	N_{symb}^{DL}	N_{symb}^{UL}
Normal CP	$\Delta f = 15$ kHz	12	7	7
Extended CP	$\Delta f = 15$ kHz	12	6	6
	$\Delta f = 7.5$ kHz	24	3	NA

of subcarriers within an RB, N_{SC}^{RB}, is 12 or 24 for the case of 15 or 7.5 kHz subcarrier spacing respectively, as shown in Table 2.3. Each element in the resource grid is called a resource element (RE) and is uniquely defined by the index pair (k, l) in a slot where $k = 0, ..., N_{RB}^{UL} \cdot N_{sc}^{RB} - 1$ and $l = 0, ..., N_{symb}^{UL} - 1$ are the indices in the FD and TD, respectively. RE (k, l) corresponds to the complex signal value $a_{k,l}$. For an RE not used for transmission of a physical channel or a physical signal in a slot, $a_{k,l}$ is set to zero. The relation between the RB index n_{RB} in the FD and RE (k, l) in a slot is given by

$$n_{RB} = \lfloor \frac{k}{N_{sc}^{RB}} \rfloor.$$

Figure 2.8 shows the detailed slot structure. We focus on the case of normal CP. The normal CP length is 5.2 μs $(160 \times T_s)$ in the first OFDM or SC-FDMA symbol and 4.7 μs $(144 \times T_s)$ in the remaining six symbols. The overhead for the normal CP setup is about 7.14%.

2.3 Downlink Distributed Transmission

The contents of this section are mainly taken from [7].
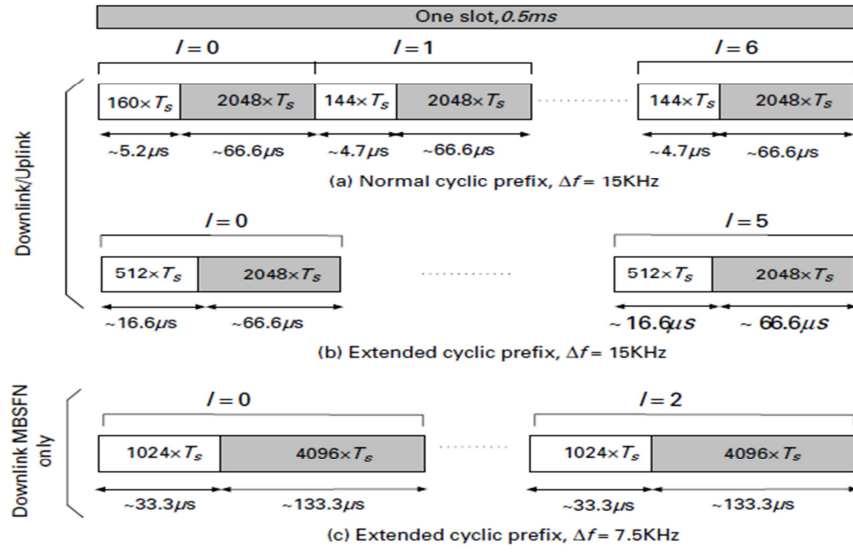
Figure 2.8: Slot structure for normal and extended CP [7, Fig. 8.3].

In the LTE DL transmission, the virtual resource block (VRB) concept is defined to enable distributed transmission. The size of VRB is same as RB. There are two types of VRBs, one is localized type, the other is distributed type. For each type of VRBs, a pair of VRBs over two time slots in a subframe is assigned together by a single virtual block number, n_{VRB}. In localized type, VRBs are mapped to RBs directly, namely $n_{RB} = n_{VRB}$. Furthermore, the VRBs of localized type are numbered from 0 to $N_{VRB}^{DL} - 1$, where $N_{VRB}^{DL} = N_{RB}^{DL}$. In the distributed type, the VRBs are numbered from 0 to $N_{VRB}^{DL} - 1$, where N_{VRB}^{DL} follows certain rules. More detailed description can be found in reference [5].

2.4   General Structure for Downlink Physical Channels

The contents of this section are mainly taken from [6]. This section gives us a brief description of the general structure of various DL physical channel defined in LTE. The baseband signal representing the physical DL channel in LTE is defined in terms of the following steps and illustrated in Figure 2.9. More detailed description can be found in reference [6].

14
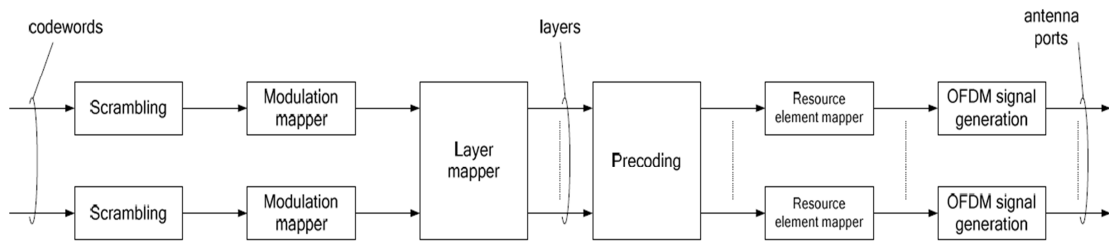
Figure 2.9: Overview of physical channel processing [6].

- Scrambling.

- Modulation of scrambled bits to generate complex-valued symbols.

- Mapping of the complex-valued modulation symbols onto one or several transmission layers.

- Transform precoding to generate complex-valued symbols.

- Precoding of the complex-valued symbols.

- Mapping of complex-valued symbols to REs.

- Generation of complex-valued time-domain OFDMA signal for each antenna port.

2.5 Reference Signal (RS)

The contents of this section are mainly taken from [7].

Three types of DL reference signals (RSs) are defined in LTE, and five types in LTE-A. They are listed below.

- Cell-specific reference signals (CRS)

- MBSFN reference signals

15

- UE-specific reference signals (DM-RS)

- Positioning reference signals (PRS) (LTE-A only)

- CSI reference signals (CSI-RS) (LTE-A only)

In this thesis, we concentrate on the cell-specific RSs.

2.5.1 Cell-Specific Reference Signals (CRS)

Cell-specific reference signals are transmitted in all DL subframes in a cell supporting non-MBSFN transmission, and are transmitted on one or several of antenna ports 0 to 3. Note that CRSs are defined for $\triangle f = 15$ only. The CRS sequence $r_{l,n_s}(m)$ is defined as

$$r_{l,n_s}(m) = \frac{1}{\sqrt{2}}(1 - 2 \cdot c(2m)) + j\frac{1}{\sqrt{2}}(1 - 2 \cdot c(2m+1)), \ m = 0, 1, ..., 2N_{PRB}^{DL} - 1, \quad (2.8)$$

where n_s and l are the slot number within a radio frame and the OFDM symbol number within the slot respectively. The pseudo-random sequence (PN sequence) is a Gold sequence composed of two sequences of length 31, which are initialized with

$$c_{init}(m) = 2^{10} \cdot (7 \cdot (n_s + 1) + l + 1) \cdot (2 \cdot N_{ID}^{cell} + 1) + 2 \cdot 2 \cdot N_{ID}^{cell} + N_{CP}, \quad (2.9)$$

at the start of each OFDM symbol where N_{ID}^{cell} is the cell identity and $N_{CP} = 1$ and 0 for normal and extended CP, respectively. The sequence $c(m)$ is defined by

$$c(m) = (x_1(m + 1600) + x_2(m + 1600)) \mod 2 \quad (2.10)$$

where $x_1(m)$ and $x_2(m)$ are respectively generated by feedback polynomials $D^{31} + D^3 + 1$ and $D^{31} + D^3 + D^2 + D + 1$ as

$$
\begin{aligned}
x_1(m + 31) &= (x_1(n + 3) + X_1(n)) \mod 2, \\
x_2(m + 31) &= (x_2(n + 3) + x_2(n + 2) + x_2(n + 1) + X_2(n)) \mod 2.
\end{aligned}
\quad (2.11)
$$
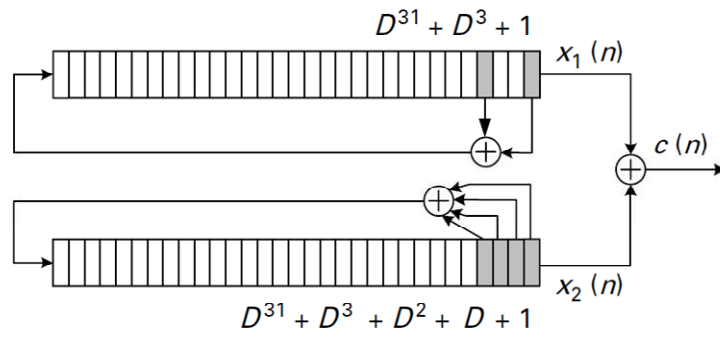
Figure 2.10: PN sequences generation in the LTE-system [7, Fig. 9.2].

The overall PN-sequences generator is illustrated in Figure 2.10.

Figure 2.11 illustrates an example of the REs used for RS transmission under normal CP. The notation R_P is used to denote an RE used for RS transmission on antenna port p.
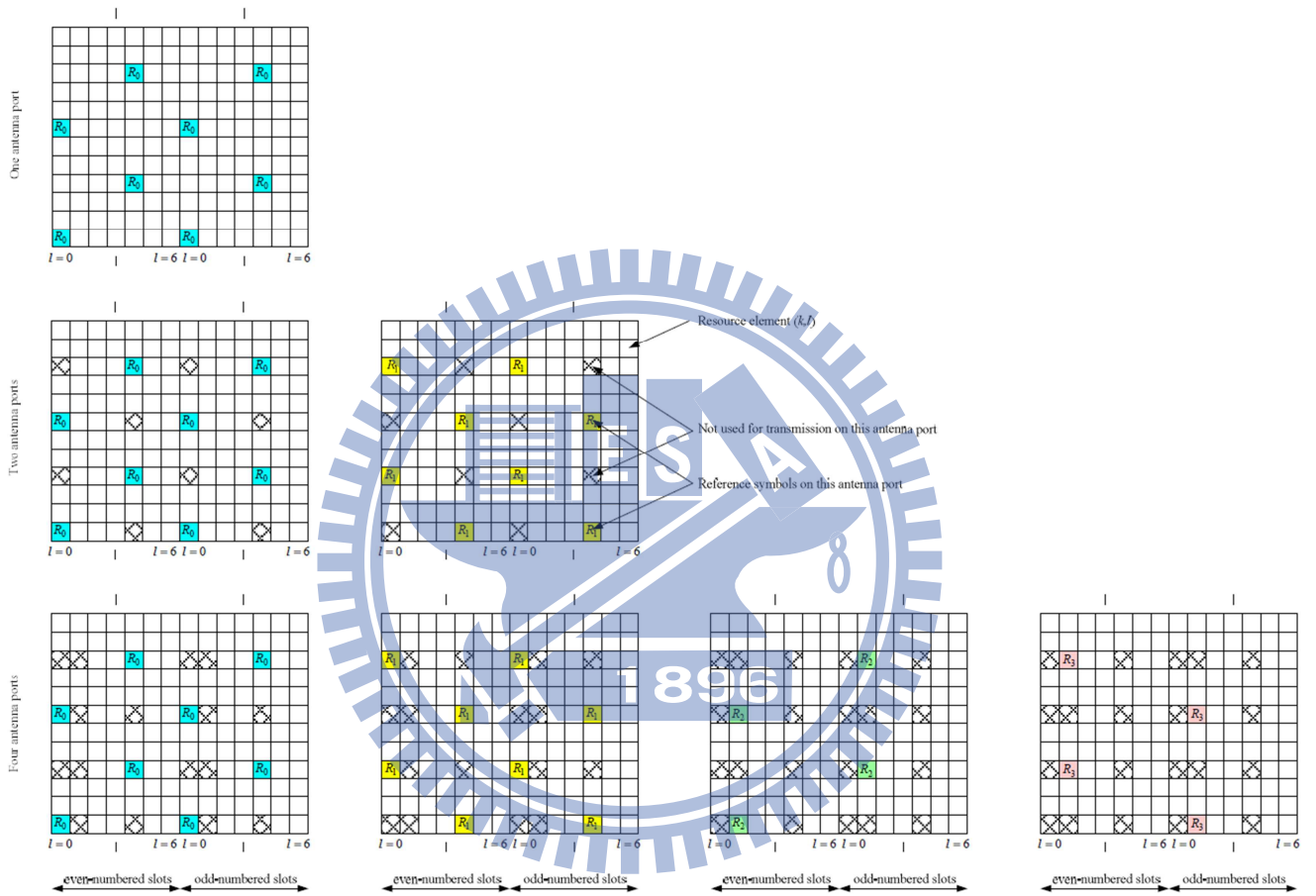
Figure 2.11: Mapping of DL RSs (normal CP) [6, Fig. 9.9].

Chapter 3

Channel Estimation Methods

Channel estimators in an OFDM or OFDMA system usually need RSs. The RS have to be transmitted continuously because a fading channel requires constant tracking. Generally speaking, the structure of the frequency response of a fading channel can be viewed as a two-dimensional (2-D) signal (frequency and time), whose values are sampled at certain positions with particular rules.

We introduce four ways of channel estimation in this chapter, including the least-squares (LS) technique, interpolation schemes, basis expansion model (BEM) with discrete prolate spheroidal sequences (DPSS), and linear minimum mean-square error (LMMSE) estimation. In the final proposal design, we use the LS technique to estimate the channel response at RSs, then use linear interpolation or BEM with DPSS in the time domain to estimate the frequency response at nonRS subcarriers within pilot symbols, and then perform LMMSE channel estimation in the frequency domain to estimate the frequency response at nonRS subcarriers within pilot symbols. Finally, we use linear interpolation or BEM with DPSS in the time domain to estimate the frequency response at nonRS subcarriers for nonpilot symbols. These building-block techniques are introduced separately in the following subsections.

3.1 Least-Squares (LS) Estimation

Based on the a priori known data, i.e., RSs, we can estimate the channel response at the RS carriers coarsely by LS estimation. Conventional LS channel estimation minimizes the squared channel estimation error based on one-sample observation [11]. Since the estimation applies to RSs in pilot symbols, we use a subscript "RS" to indicate it. The minimization objective is given by

$$\|Y_{RS,P} - \hat{H}_{RS,P,LS} \cdot X_{RS,P}\|^2, \tag{3.1}$$

where $Y_{RS,P}$ is the received RS in pilot symbols after passing through the channel and $X_{RS,P}$ is the a priori known RS in pilot symbols, both in the FD and both being $M \times 1$ vectors and can be written as

$$Y_{RS,P} = [Y_{RS,P}(0) \; Y_{RS,P}(1) \; ... \; Y_{RS,P}(N_P - 1)]^T, \tag{3.2}$$

$$X_{RS,P} = [X_{RS,P}(0) \; X_{RS,P}(1) \; ... \; X_{RS,P}(N_P - 1)]^T, \tag{3.3}$$

where N_P is the RS subcarrier numbers within the pilot symbol. $\hat{H}_{RS,P,LS}$ is an $N_P \times N_P$ diagonal matrix as

$$\hat{H}_{RS,P,LS} = \begin{bmatrix} \hat{H}_{RS,P,LS}(0) & ... & 0 & ... \\ 0 & \hat{H}_{RS,P,LS}(1) & 0 & ... \\ 0 & ... & \hat{H}_{RS,P,LS}(2) & ... \\ 0 & ... & 0 & \hat{H}_{RS,P,LS}(N_P - 1) \end{bmatrix}. \tag{3.4}$$

The LS channel estimate at RS subcarrier k, based on one observed OFDMA symbol $Y_{RS,P}$ only, is given by

$$\hat{H}_{RS,P,LS}(k) = \frac{Y_{RS,P}(k)}{X_{RS,P}(k)} = H_{RS,P} + Z(k)/X_{RS,P}(k), \tag{3.5}$$

where $k = 0, ..., N_P - 1$, and $Z(k)$ is the complex white Gaussian noise at RS subcarrier k.

20

3.2 Linear Interpolation

After obtaining the channel response estimates at some distributed subcarriers in frequency and in time, we may use interpolation to estimate the channel responses for the subcarriers between them. Linear interpolation is a commonly considered scheme due to its low complexity. It does interpolation between two known data. For example, we may use the channel information at two RS subcarriers in pilot symbols obtained by the LS estimator to estimate the channel frequency responses at the data symbols between them. We may also use linear extrapolation to estimate the responses at the data beyond the outermost RSs.

Mathematically, suppose we have two points (x_1, y_1) and (x_2, y_2) that are assumed to satisfy a linear relation as

$$aX + b = Y, \tag{3.6}$$

where a and b are unknown. Then we have

$$ax_1 + b = y_1, \ ax_2 + b = y_2.$$

We can write the equations in matrix form as

$$\begin{bmatrix} x_1 & 1 \\ x_2 & 1 \end{bmatrix} \begin{bmatrix} a \\ b \end{bmatrix} = \begin{bmatrix} y_1 \\ y_2 \end{bmatrix}. \tag{3.7}$$

Then the unknown parameters a and b can be solved as

$$\begin{bmatrix} a \\ b \end{bmatrix} = \begin{bmatrix} x_1 & 1 \\ x_2 & 1 \end{bmatrix}^{-1} \begin{bmatrix} y_1 \\ y_2 \end{bmatrix} = \frac{1}{x_2 - x_1} \begin{bmatrix} y_2 - y_1 \\ x_2 y_1 - x_1 y_2 \end{bmatrix}. \tag{3.8}$$

When the above interpolation is carried out in the TD between two pilot symbols at the same subcarrier, the idea is as illustrated in Figure 3.1.

3.3 Discrete Prolate Spheroidal Sequences (DPSS)

The contents of this section are mainly taken from [12].

21
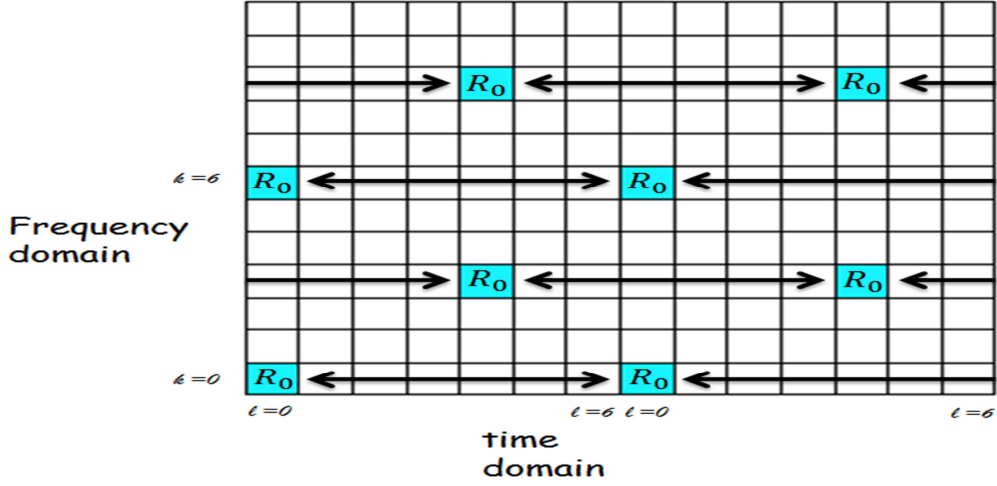
Figure 3.1: Illustration of linear interpolation in TD.

Slepian [13] introduced sequences which are bandlimited to the frequency domain $[-v_{Dmax},\ v_{Dmax}]$ and furthermore most concentrated in a certain time interval of length M. The quantity v_{Dmax}, denoting the maximum normalized Doppler bandwidth, is defined as

$$v_{Dmax} = \frac{v_{max} f_C}{c_0} T_{sym},\tag{3.9}$$

where v_{max} is the maximum velocity, T_{sym} is the OFDM symbol duration, and c_0 is the light speed. Consider a sequence $u[m]$ bandlimited to v_{Dmax} so that

$$u[m] = \int_{-v_{Dmax}}^{v_{Dmax}} U(v) e^{j2\pi mv} dv,\tag{3.10}$$

where

$$U[v] = \sum_{m=-\infty}^{\infty} u[m] e^{-j2\pi mv},\tag{3.11}$$

while having its maximum energy concentration in an interval of length M

$$\lambda(v_{Dmax}, M) = \frac{\sum_{m=0}^{M-1} |u[m]|^2}{\sum_{m=-\infty}^{\infty} |u[m]|^2}.\tag{3.12}$$

The solution for the optimization problems (3.12) is the discrete prolate spheroidal sequences

22

(DPSS). The ith DPSS $u_i[l, v_{Dmax}, M]$ is defined as the real solution of

$$\sum_{l=0}^{M-1} \frac{\sin(2\pi v_{Dmax}(l-m))}{\pi(l-m)} u_i[l, v_{Dmax}, M] = \lambda_i(v_{Dmax}, M) u_i[m, v_{Dmax}, M], \qquad (3.13)$$

for $i \in \{0, ..., M-1\}$ and $m \in \{-\infty, ..., \infty\}$ [12]. We drop the arguments v_{Dmax} and M from $\lambda_i(v_{Dmax}, M)$ below for simplicity.

The DPSS are doubly orthonormal on the infinite set $\{-\infty, ..., \infty\} \triangleq \mathbb{Z}$ as well as the finite set $\{0, ..., M-1\}$ as

$$\sum_{m=0}^{M-1} u_i[m]u_j[m] = \lambda_i \sum_{-\infty}^{\infty} u_i[m]u_j[m] = \delta_{ij}, \qquad (3.14)$$

where $i, j \in \{0, ..., M-1\}$. The eigenvalues λ_i associated with the sequences $u_i[m]$ have following properties [12]:

- λ_i is near 1 for $i \leq \lceil 2v_{Dmax}M \rceil + 1$.

- λ_i drops to zero rapidly for $i > \lceil 2v_{Dmax}M \rceil + 1$.

Hence the dimension of the signal space is approximately given by

$$D' = \lceil 2v_{Dmax}M \rceil + 1. \qquad (3.15)$$

For the purpose of channel estimation, the index set $m \in \{0, ..., M-1\}$, where m may be taken to be the OFDM symbol number. The DPSS expands the sequence $H[m]$ by

$$H[m] \approx \tilde{H}[m] = \sum_{i=0}^{D-1} u_i[m]\gamma_i, \qquad (3.16)$$

where γ_i is the weighting coeffieients of the Slepian sequence, and the dimension D has the constraints

$$D' \leq D \leq M. \qquad (3.17)$$
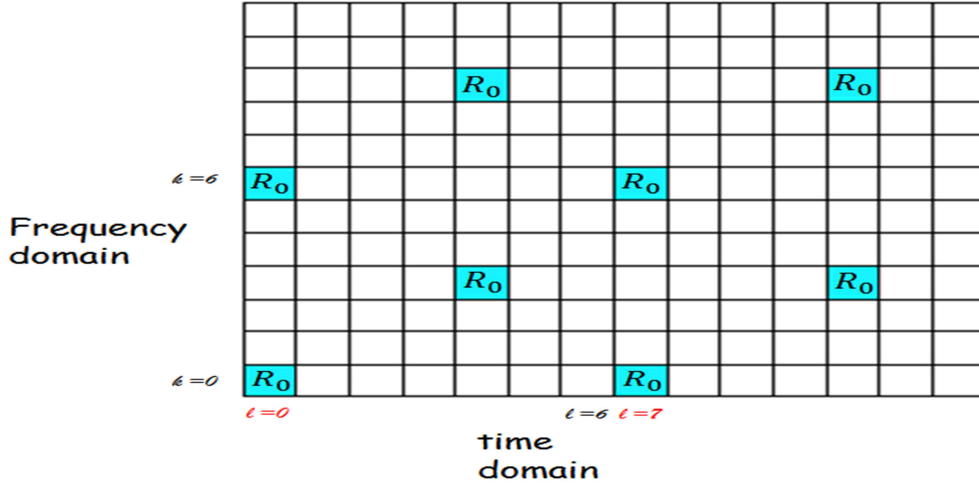
Figure 3.2: Illustration of $\mathbb{P}_k$.

The weighting coefficient γ_i for $i \in \{0, ..., D-1\}$ is calculated as

$$\gamma_i \approx \hat{\gamma}_i = \sum_{m=0}^{M-1} \hat{H}[m] u_i^*[m], \tag{3.18}$$

where $\hat{H}[m]$ can be derived by the LS method at RS subcarriers.

In the LTE DL, RSs are only located at some OFDM symbols $m \in \mathbb{P}_k$, where $\mathbb{P}_k$ is the set of positions of RSs for subcarrier k. As depicted in Figure 3.2, $\mathbb{P}_0$ is composed by OFDM symbol number $l = 0$ and $l = 7$ for subcarrier index $k = 0$. For simplicity, we consider a fixed subcarrier k and omit the index k in the next paragraph.

The orthogonality of the Slepian sequences is lost by only taking some values of m. In order to correct the loss of orthogonality, we have to introduce a matrix $\mathbf{G}$ as

$$\mathbf{G} = \sum_{m \in \mathbb{P}} \mathbf{f}[m] \mathbf{f}^H[m], \tag{3.19}$$

where

$$\mathbf{f}[m] = \begin{bmatrix} u_0[m] \\ \cdot \\ \cdot \\ u_{D-1}[m] \end{bmatrix}. \tag{3.20}$$

24

The corrected $\hat{\gamma}$ can be derived as [12]

$$\hat{\gamma} = \mathbf{G}^{-1} \sum_{m \in \mathbb{P}} \hat{H}[m]\mathbf{f}^*[m],$$
(3.21)

where

$$\hat{\gamma} = \begin{bmatrix} \hat{\gamma}_0 \\ \cdot \\ \cdot \\ \cdot \\ \hat{\gamma}_{D-1} \end{bmatrix}.$$
(3.22)

Finally, we can use (3.16) to expand the sequences for $m \notin \mathbb{P}_k$.

3.4 Linear Minimum-Mean Square Error (LMMSE) Channel Estimation

The linear minimum mean square error (LMMSE) estimator uses second-order statistics about the channel and the noise to reduce the amount of noise in an existing channel estimate, such as the LS channel estimate, as

$$\hat{H}_{RS,LMMSE} = R_{H_{RS}H_{RS,P}}[R_{H_{RS,P}H_{RS,P}} + \sigma_z^2 (X_{RS,P}^H X_{RS,P})]^{-1}\hat{H}_{RS,P,LS},$$
(3.23)

where $\hat{H}_{RS,P,LS}$ is the LS estimate vector obtained as in (3.5), σ_z^2 is the variance of AWGN, $R_{H_{RS,P}H_{RS,P}}$ is the autocorrelation matrix of the RS subcarriers within the same pilot symbol, $R_{H_{RS}H_{RS,P}}$ is the crosscorrelation matrix between all subcarriers and the subcarriers with the RSs within the same pilot symbol, and the superscript $(\cdot)^H$ denotes Hermitian transpose. By replacing the term $(X_{RS,P}^H X_{RS,P})$ in (3.23) with its expectation $E[(X_{RS,P}^H X_{RS,P})]$, the LMMSE channel estimator in frequency domain can be represented as

$$\hat{H}_{RS,LMMSE} = R_{H_{RS}H_{RS,P}}(R_{H_{RS,P}H_{RS,P}} + \frac{\beta}{SNR}I)^{-1}\hat{H}_{RS,P,LS},$$
(3.24)

where β is a constant depending on the type of modulation, SNR is the average signal-to-noise ratio and I is the identity matrix with same size as $R_{H_{RS,P}H_{RS,P}}$.

As mentioned in chapter 1, we can approximate $R_{H_{RS}H_{RS,P}}$ and $R_{H_{RS,P}H_{RS,P}}$ by the mean delay (τ_μ) and the RMS delay spread (τ_{rms}). The mean delay and the RMS delay spread are given by, respectively,

$$\tau_\mu = \frac{\sum_{l=0}^{L-1} |\overline{\alpha_l}|^2 l}{\sum_{l=0}^{L-1} \|\overline{\alpha_l}\|^2} \tag{3.25}$$

and

$$\tau_{rms} = \sqrt{\frac{\sum_{l=0}^{L-1} |\overline{\alpha_l}|^2 (l - \tau_\mu)^2}{\sum_{l=0}^{L-1} |\overline{\alpha_l}|^2}}. \tag{3.26}$$

One question here is how the time domain averaging ($|\overline{\alpha_l}|^2$) should be defined. As our purpose is channel estimation, suppose one channel estimation is performed for K pilot symbols. Then the expectation should be an average taken over these symbols. In the extreme case of $K = 1$, no average should be taken, but the instantaneous channel response in that symbol period should be used to compute τ_μ and τ_{rms}.

Once we get τ_μ and τ_{rms}, the elements of crosscorrelation matrix and autocorrelation matrix can be defined if we assume the channel has exponential PDP. For an exponential PDP with possibly nonzero initial delay τ_0, we have

$$\frac{R_f(k)}{R_f(0)} = \frac{e^{-j2\pi\tau_0 k/N}}{1 + j2\pi\tau_{rms}k/N}, \tag{3.27}$$

where $\tau_0 = \tau_\mu - \tau_{rms}$ and N is the FFT size used in the multicarrier system.

3.4.1 Estimation of Channel Delay Parameters

Method 1 ("K")

The material in this section is mainly taken from [2].

If we advance the channel response by (an arbitrary) τ time units, then the frequency response becomes

$$H_a(f) = e^{j2\pi\tau f/N}H(f) = \sum_{l=0}^{L-1} \alpha_l(l - \tau)e^{-j2\pi(l-\tau)f/N}. \tag{3.28}$$

Differentiating $H_a(f)$ with respect to f, we get

$$\frac{dH_a(f)}{df} = \frac{-j2\pi}{N} \sum_{l=0}^{L-1} \alpha_l(l-\tau)e^{-j2\pi(l-\tau)f/N}. \tag{3.29}$$

Applying Parseval's theorem, we get

$$\left\langle |\frac{dH_a(f)}{df}|^2 \right\rangle = \frac{4\pi^2}{N^2} \sum_{l=0}^{L-1} |\alpha_l|^2(l-\tau)^2, \tag{3.30}$$

where $< \cdot >$ means frequency averaging. Taking average over time, we get

$$\overline{\left\langle |\frac{dH_a(f)}{df}|^2 \right\rangle} = \frac{4\pi^2}{N^2} \sum_{l=0}^{L-1} |\overline{\alpha_l}|^2(l-\tau)^2 \triangleq \overline{J}(\tau), \tag{3.31}$$

where the overline $\overline{\cdot}$ indicates time averaging. The above equations show that $\overline{J}(\tau)$ is minimized when $\tau = \tau_\mu$. In addition,

$$\tau_{rms}^2 = \frac{N^2 \min \overline{J}(\tau)}{4\pi^2 \sum_{l=0}^{L-1} |\overline{\alpha_l}|^2}. \tag{3.32}$$

We can estimate τ_μ and τ_{rms} in this way, and it is suitable for typical pilot-aided OFDMA systems.

Consider a system where one out of every F_s subcarriers is a RS. Later, we will see that how F_s can be set in LTE. We can approximate $dH_a(f)/df$ by first-order difference, say, $[H_a(f + F_s) - H_a(f)]/F_s$, and substitute it into (3.31). Then, we obtain

$$\overline{J}(\tau) \approx \frac{1}{F_s^2} \overline{\left\langle |e^{j\phi}H(f + F_s) - H(f)|^2 \right\rangle_p}, \tag{3.33}$$

where $\phi = 2\pi\tau F_s/N$, f takes values only over RS frequencies, and $< \cdot >_p$ denotes averaging over RS subcarriers. By sampling theory, it is proper to take circular differencing over f rather than linear differencing [2]. Therefore, we approximate $\overline{J}(\tau)$ by

$$\overline{J}(\tau) \approx \frac{1}{F_s^2} \overline{\left\langle |e^{j\phi}H((f + F_s)\%N) - H(f)|^2 \right\rangle_p}, \tag{3.34}$$

where % denotes modulo operation, $< \cdot >_p$ now averages over the full number of RS sub-carriers, and we have assumed that $(f + F_s)\%N$ is an RS subcarrier. Now let R_i be the frequency-domain autocorrelation of the channel response as

$$R_i = \left\langle H((f + iF_s)\%N)H^*(f) \right\rangle_p. \tag{3.35}$$

Then from (3.34) we have

$$\overline{J}(\tau) \approx \frac{2}{F_s^2}[\overline{R}_0 - \Re\{e^{j\phi}\overline{R}_1)\}]. \tag{3.36}$$

Thus (3.36) gives an approximation of $\overline{J}(\tau)$. According to (3.36), τ_μ and τ_{rms} can be estimated in the following way:

1. estimate the channel responses at the RS subcarrier,

2. estimate R_i $(i = 0, 1)$,

3. estimate $\overline{J}(\tau)$,

4. find the value of τ that minimizes $\overline{J}(\tau)$,

5. substitute the min $\overline{J}(\tau)$ into (3.32) to estimate τ_{rms}^2, and

6. estimate τ_0.

Step 1 can be achieved using the LS method. Then, in step 2, R_0 and R_1 can be estimated via

$$\hat{R}_0 = \left\langle |\hat{H}(f)|^2 \right\rangle_p - \hat{\sigma}_n^2, \quad \hat{R}_1 = \left\langle \hat{H}(f + F_s\%N)\hat{H}^*(f) \right\rangle_p, \tag{3.37}$$

where $\hat{H}(f)$ denotes the estimated channel response at RS subcarrier f and, we may obtain the noise power $\hat{\sigma}_n^2$ from the received power in the null subcarriers of the system. Thus, for step 3, $\overline{J}(\tau)$ can be estimated using

$$\overline{\hat{J}}(\tau) \triangleq \frac{2}{F_s^2}\left[\overline{\hat{R}_0} - \Re\{e^{j\phi}\overline{\hat{R}_1}\} \right]. \tag{3.38}$$

28

If one performs a channel estimation over K pilot symbols, then the averages should be taken over these K symbols. If $K = 1$, then the instantaneous values should be used instead of averages. For step 4, we may estimate the mean delay as

$$\hat{\tau}_\mu \triangleq \arg\min \overline{\hat{J}(\tau)} = -\frac{N\angle\overline{\hat{R}_1}}{2\pi F_s}, \tag{3.39}$$

which also yields $\min \hat{J}_{Av}(\tau) = 2[\overline{\hat{R}_0} - |\overline{\hat{R}_1}|]/F_s^2$. For step 5, in view of (3.32) and that $R_0 = < |H(f)|^2 >_p$, we may estimate τ_{rms} as

$$\hat{\tau}_{rms} = \frac{N}{2\pi F_s} \sqrt{2\Big[1 - \frac{|\overline{\hat{R}_1}|}{\overline{\hat{R}_0}}\Big]}. \tag{3.40}$$

Finally, the initial delay τ_0 can be estimated via

$$\hat{\tau}_0 = \hat{\tau}_u - \hat{\tau}_{rms}. \tag{3.41}$$

Method 2 ("Y")

Recall (3.27). We can get

$$\frac{R_f(k)}{R_f(0)} \times (1 + j2\pi\tau_{rms}k/N) = e^{-j2\pi\tau_0 k/N}. \tag{3.42}$$

For convenience, let

$$R = \frac{R_f(k)}{R_f(0)} \tag{3.43}$$

and

$$X = \frac{2\pi\tau_{rms}k}{N}. \tag{3.44}$$

Substituting (3.43) and (3.44) into (3.42) yields

$$R \times (1 + jX) = e^{-j2\pi\tau_0 k/N}. \tag{3.45}$$

Taking the squared magnitudes of both sides of (3.45) yields

$$1 = |R \times (1 + jX)|^2$$
$$= (\Re(R) - \Im(R)X)^2 + (\Im(R) - \Re(R)X)^2 \tag{3.46}$$
$$= (\Re(R)^2 + \Im(R)^2)(1 + X^2).$$

To solve for X, we rewrite (3.46) as

$$
\begin{aligned}
X^2 &= \frac{1}{\Re(R)^2 + \Im(R)^2} - 1 \\
&= \frac{R_f(0)^2}{\Re(R_f(k))^2 + \Im(R_f(k))^2} - 1.
\end{aligned}
\tag{3.47}
$$

The above equation have several unknowns, which are k and $R_f(k)$. As in method 1, we can replace k by F_s for a system where one out of every F_s subcarriers is a RS. The other unknown $R_f(k)$ can be derived by (3.37), too. As a result, we get from (3.44) and (3.47) that

$$
\hat{\tau}_{rms} = \frac{N}{2\pi F_s} \sqrt{\frac{\hat{R}_0^{\,2}}{\Re(\hat{R}_1)^2 + \Im(\hat{R}_1)^2} - 1}.
\tag{3.48}
$$

We substitute the result back to (3.42). Finally, we may estimate τ_0 by

$$
\hat{\tau}_0 = \frac{-\angle(\frac{\hat{R}_1}{\hat{R}_0} \times (1 + j2\pi\hat{\tau}_{rms}F_s/N))}{2\pi F_s/N}.
\tag{3.49}
$$

3.5 Improving the Accuracy of the Estimated Channel Parameters

The question which we must consider is accuracy of our estimated channel parameters. In an LTE system, the distance between adjacent CRSs in the frequency domain is 6 subcarriers or 90 kHz, which is on the order of coherence bandwidths of outdoor channels that have middle to large spreads. To improve the accuracy of the estimated channel parameters, shorten the distances between adjacent RSs can be considered. However, the distance is set by LTE which we cannot violate, so we consider producing "pseudo" RR by linear interpolation or use of BEM with DPSS in TD of channel response estimates at the RS subcarriers in some other pilot symbols. The idea is illustrated in Figure 3.3, where R_0 is channel response at the RS subcarriers, and P_0 is a pseudo RR that is estimated via linear interpolation or BEM with DPSS. The pseudo RR can be treated similarly as the original channel response at the
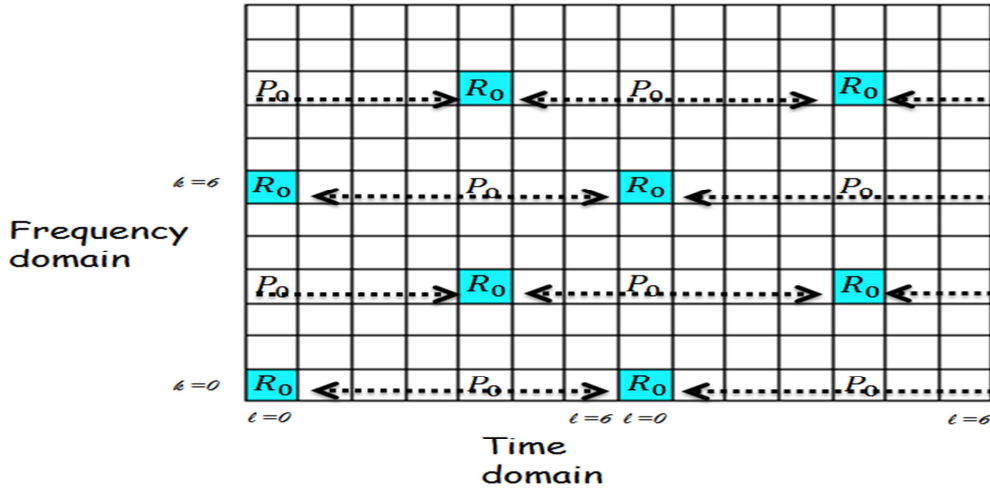
Figure 3.3: Illustration of pseudo RR.

RS subcarriers in channel estimation, which makes the distance between adjacent RSs in the FD reduced. In Figure 3.3, the distance between adjacent RSs in the FD is 6 originally, but now can be made to equal 3.

3.5.1 Channel Estimation Flow

With the idea of producing pseudo RR, the overall channel estimation flow is depicted in Figure 3.4. In Figure 3.4(a), we use the LS in FD to estimate RSs then we get R_0. In Figure 3.4(b), we produce some P_0 by linear interpolation or use of BEM with DPSS in TD of channel response estimates at the RS subcarriers in some other pilot symbols. In Figure 3.4(c), the channel delay parameters can be estimated via R_0 and P_0. The estimated channel delay parameters can be substituted into proper places in (3.27) then the resulting autocorrelation function and crosscorrelation function of channel frequency response can be used in the LMMSE channel estimate. Note that we only use the LMMSE method in FD, thus we can get other data, denoted as D, only in pilot symbols. In Figure 3.4(d), we estimate remaining data signals via linear interpolation or use of BEM with DPSS in TD of
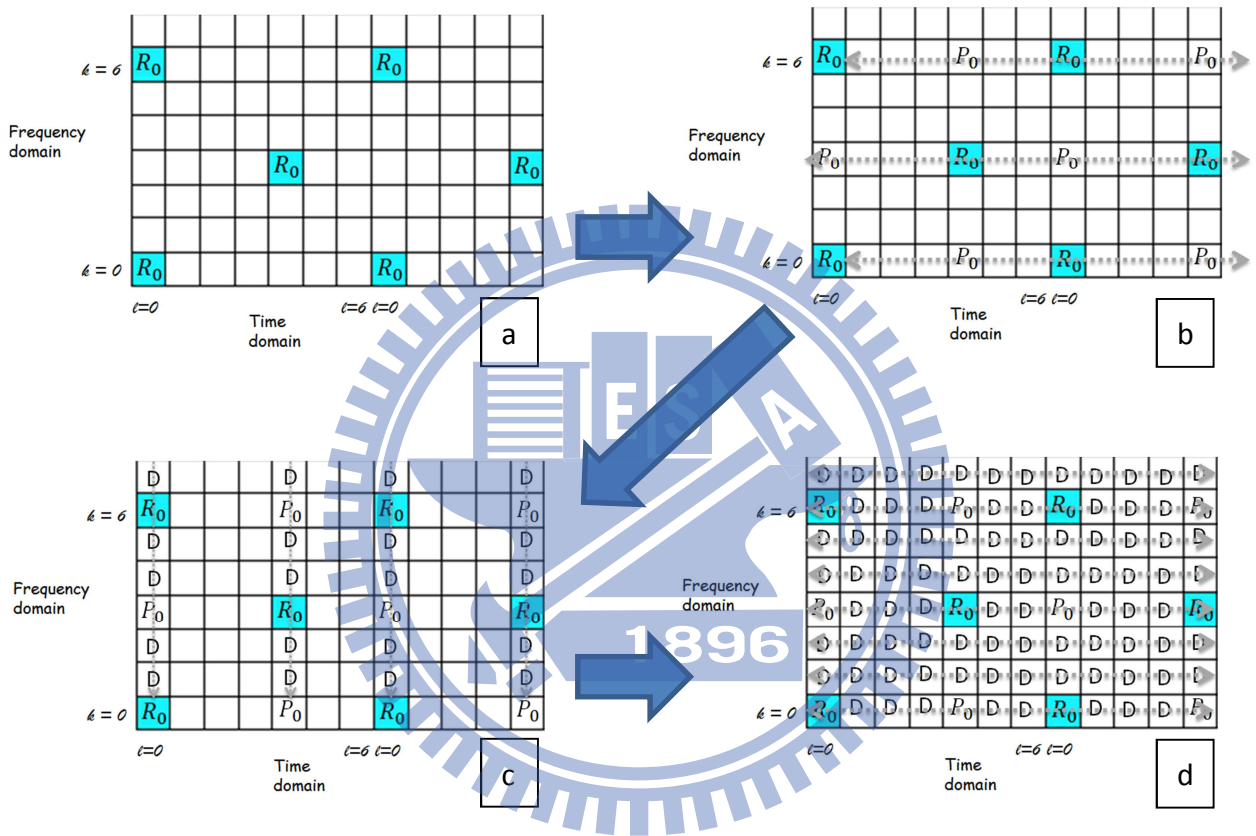
31

Figure 3.4: Channel estimation flow with use of pseudo RR.

channel response estimates at the data subcarriers in notpilot symbols.

Chapter 4

Simulation of LTE Downlink Channel Estimation

In this chapter, we take the LMMSE approach described in the last chapter to do LTE DL channel estimation. We evaluate the performance of different ways of channel estimation quantitatively using the mean square error (MSE) and symbol error rate (SER).

4.1 Simulation Conditions

The system parameters used in our simulation are listed in Table 4.1. In addition to AWGN which is for calibration purpose, we also simulate SUI-2 (where SUI stand for Stanford University Interim),SUI-4, SUI-5, TU (Typical Urban) [10], ITU-VA (International Telecommunication Union Radiocommunication Vehicular A), and an artificial channel model based on ITU-VA [2]. The SUI channels model deal suburban path loss environments in three different types, depending on the tree density and pass loss condition. The three types in suburban area are listed in Table 4.2. SUI1 and SUI2 are Rician multipath channels and the other four are Rayleigh multipath channels; the former two correspond to situations with line-of-sight (LOS) and the latter four non LOS respectively. The Rayleigh channels are more hostile and exhibit a greater root-mean-square (RMS) delay spread. In our simulation, we employ

Table 4.1: OFDMA Downlink Parameters (Normal CP)

Parameters	Values
Bandwidth [MHz]	5 / 10
modulation type	QPSK
Central frequency [GHz]	2
Number of resource blocks	25 / 50
Number of occupied subcarriers	300 / 600
CP time [μs] (first symbol in slot, else)	5.2, 4.7
N_{FFT}	512/1024
Sampling frequency [MHz]	7.68 / 15.36
Subcarrier spacing [kHz]	15
Symbol time [μs] (first symbol in slot, else)	71.8, 71.3
Samples per slot	3840 / 7680

three types of environments, i.e., terrain A, B, and C. We select SUI-2, SUI-4, and SUI-5 as representative for terrain C, terrain B, and terrain A, respectively. For simplicity, we use Rayleigh fading to model SUI-2 instead of Rician fading.

The TU channel model, as its name shows, is a channel model for the urban environment. The TU channel model is also a Rayleigh channel, but there are 12 taps in it, which is four-times that of SUI channels. The ITU-VA is a channel model for UE in vehicular type of motion. The ITU-VA channel model is a Rayleigh channel. There are 6 taps in it, which is two-times that of SUI channels. In order to see how the proposed technique may perform in various conditions, we choose these quite different channel models to do our simulation. Artificial ITU-VA [2], the PDP of which is far from exponential PDP, is also chosen to see how the proposed technique may perform when the PDP is totally different from exponential PDP. The PDP of the artificial ITU-VA consists of three copies of ITU-VA's PDP with intercluster delays of 2 and 4 μs, respectively. The relative power scales of three clusters are 0, 5, and −2 dB, respectively. It has been shown that exponential PDP modeling performs better than uniform modeling [2] when the PDP is Artificial ITU-VA. But the performance is unknown for exponential PDP modeling in the method described in chapter 3. We thus
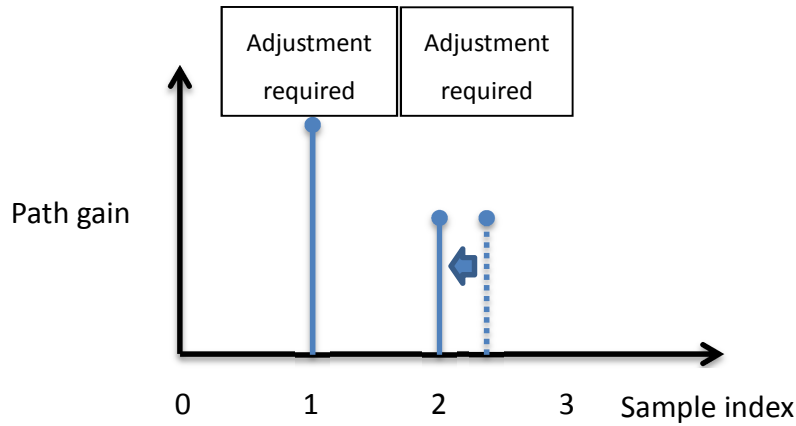
Figure 4.1: Tap adjustment.

Table 4.2: SUI Channel Model for Differetn Terrain Types

Terrain type	Description	SUI channels
A	hilly terrain with heavy tree	SUI5, SUI6
B	flat terrain with heavy tree, hilly terrain with light tree	SUI3, SUI4
C	flat terrain with light tree	SUI1, SUI2

simulate this channel model to understand it.

Tables 4.3–4.8 present the characteristics of the models mentioned above. Note that the PDP of each channel model may not have the path delays equal to integer multiples of the LTE sample spacing. Experience with the Matlab channel simulator shows that this situation results in huge amount of memory usage which causes difficulty in simulation of systems where the FFT size is more than 512. To solve this problem, the PDP listed in Table 4.4–4.8 are adjusted by forcing each channel impulse response tap to its nearest sampling point by rounding to preserve the path number as well as path power. The idea is illustrated in Figure 4.1. Expeiments show that the performance with and without tap adjustment is almost the same.

Table 4.3: PDP of SUI2

Tap	Relative delay		Average power	
	μs	sample numbers (512,1024)	dB	normalized dB
1	0	(1, 1)	0	−0.393
2	0.4	(4, 7)	−12	−12.393
3	1.1	(9, 18)	−15	−15.393

Table 4.4: PDP of SUI4

Tap	Relative delay		Average power	
	μs	sample numbers (512,1024)	dB	normalized dB
1	0	(1, 1)	0	−1.9218
2	1.5	(13, 24)	−4	−5.9218
3	4	(32, 62)	−8	−9.9218

Table 4.5: PDP of SUI5

Tap	Relative delay		Average power	
	μs	sample numbers (512,1024)	dB	normalized dB
1	0	(1, 1)	0	−1.5113
2	4	(32, 62)	−5	−6.5113
3	10	(78, 155)	−10	−11.5113

4.1.1 Parameter Setting

We now discuss considerations concerning tap number of LMMSE filtering, length of DPSS, time-bandwidth product, and number of DPSS bases.

It is known that the coherent bandwidth, denoted as B_c herein, is inversely proportional

Table 4.6: PDP of TU

| | Relative delay | | Average power | |
Tap	μs	sample numbers (512,1024)	dB	normalized dB
1	0	(1, 1)	-4	-10.3582
2	0.1	(2, 3)	-3	-9.3582
3	0.3	(3, 6)	0	-6.3582
4	0.5	(5, 9)	-2.6	-8.9582
5	0.8	(7, 13)	-3	-9.3582
6	1.1	(9, 18)	-5	-11.3582
7	1.3	(11, 21)	-7	-13.3582
8	1.7	(14, 27)	-5	-11.3582
9	2.3	(19, 36)	-6.5	-12.3582
10	3.1	(25, 49)	$-.6$	-14.9582
11	3.2	(26, 50)	-11	-17.3582
12	5.0	(39, 78)	-10	-16.3582

Table 4.7: PDP of ITU-VA

| | Relative delay | | Average power | |
Tap	μs	sample numbers (512,1024)	dB	normalized dB
1	0	(1, 1)	0	-3.14
2	0.31	(3, 6)	-1	-4.14
3	0.71	(6, 12)	-9	-12.14
4	1.09	(9, 18)	-10	-13.14
5	1.73	(14, 28)	-15	-18.14
6	2.51	(20, 40)	-20	-23.14

to the RMS delay spread denoted τ_{rms}, that is [10],

$$B_c \propto \frac{1}{\tau_{rms}}. \qquad (4.1)$$

The proportionality constant in (4.1) may vary with the definition of coherence bandwidth or other considerations. For instance, if the coherence bandwidth is defined as bandwidth

Table 4.8: PDP of Artificial ITU-VA

Tap	Relative delay		Average power	
	μs	sample numbers (512,1024)	dB	normalized dB
1	0	(1, 1)	0	−9.95
2	0.31	(3, 6)	−1	−10.95
3	0.71	(6, 12)	−9	−18.95
4	1.09	(9, 18)	−10	−19.95
5	1.73	(14, 28)	−15	−24.95
6	2	(16, 32)	5	−4.95
7	2.31	(19, 36)	4	−5.95
8	2.51	(20, 40)	−20	−29.95
9	2.71	(22, 43)	−4	−13.95
12	3.09	(25, 48)	−5	−14.95
11	3.73	(30, 58)	−10	−19.95
12	4	(32, 62)	−2	−11.95
13	4.31	(34, 67)	−3	−12.95
14	4.51	(36, 70)	−15	−24.95
15	4.71	(37, 73)	−11	−20.95
16	5.09	(40, 79)	−12	−21.95
17	5.73	(45, 89)	−17	−26.95
18	6.51	(51, 101)	−22	−31.95

Table 4.9: RMS Delay of Channel after Tap Adjustment with FFT size = 512

Channel Model	SUI-2	SUI-4	SUI-5	TU	ITU-VA	Artificial ITU-VA
RMS delay spread (sample)	1.485	9.794	21.92	7.905	2.726	9.437
RMS delay spread (μs)	0.193	1.275	2.854	1.03	0.355	1.229

with correlation of 0.9 or above in channel frequency response, then we have

$$B_c \approx \frac{1}{50\tau_{rms}}. \tag{4.2}$$

In case the coherence bandwidth is defined as bandwidth with correlation of 0.5 or above in

channel frequency response, it is given as

$$B_c \approx \frac{1}{5\tau_{rms}}. \tag{4.3}$$

Here we consider the latter definition. In this case, if τ_{rms} is equal to 2 μs, which is a relatively large RMS delay spread, then the coherence bandwidth is equal to 100 kHz. On the other hand, if τ_{rms} is equal to 0.2 μs, which is a relatively small RMS delay spread, then the coherence bandwidth is equal to 1 MHz. The use of pseudo RR as discussed in chapter 3 makes the spacing between adjacent RSs equal to 45 kHz in LTE and LTE-A. Considering both the large and small RMS delay spread environments, it appears that 4 is a proper number of LMMSE filter taps.

Now consider the other parameters, namely, length of DPSS, time-bandwidth product, and number of DPSS bases. We may intuitively expect that a longer length of the DPSS should result in better performance. But longer DPSS imply grater latency and grater memory requirement. We let it be 7 slots plus 1 symbol, i.e., about 3.6 ms in our simulation, which is a relatively arbitrary choice. The time-bandwidth product is related to the normalized Doppler frequency, which is not estimated in this thesis. But as shown in (3.15), the product has to be rounded in determining the dimensions used, which means there is a high tolerance to error in the assumed normalized Doppler frequency. Our simulation results show that DPSS for higher normalized Doppler frequencies can be used in cases with lower normalized Doppler frequencies with some small degradation. Thus we choose a set that corresponds to about 150–300 km/h for the 0-300 km/h operating environment when the carrier frequency is equal to 2 GHz. The number of DPSS bases, where each basis sequence corresponds to a different eigenvalue, is determined by simulation. We find that eigenvalues lower than 0.001 can be discarded with little degradation. And the lowest eigenvalue should be in the interval [0.01, 0.001] for the best performance. So here we preserve 7 DPSS bases, where the 7th eigenvalue is 0.0034 and the 8th is 0.00018.

4.2 Simulation Results for LTE

In our simulation, we assume perfect synchronization. We also assume that the channels are block-static, i.e., they have constant responses within one symbol duration.

Because we simulate many different ways of channel estimation, each figure will contain many lines. We here give a brief outline of the different methods and how their corresponding results are indicated in the figures. There are 16 lines in each figure, each line representing a certain method. The lines are named ALS, Interp, PerPL, KML, YML, YD-MA, KD-MA, YDMD, KDMD, YDML, KDML, PerPD, YL-MA, KL-MA, YLML and KLML. ALS means perfect condition. where all subcarriers in all symbols are RSs. This condition is used as a reference condition for performance comparison. PerP is similar to ALS, the only difference being that all subcarriers are RSs in pilot symbols only. "L" means doing linear interpolation/extrapolation in time domain. "K" and "Y" are method 1 and method 2, respectively, as introduced in Section 3.4.1, which are different methods to estimate the channel delay parameters. "D" means using BEM with DPSS in TD. "M" means doing LMMSE estimation in FD on pilot symbols only, whereas "MA" means doing LMMSE estimation in FD on all symbols.

A brief describtion of the various different methods are as follows.

1) ALS:

- Estimate the channel response at each subcarriers by the LS technique.

2) PerPL and PerPD:

- Estimate the channel response at each RS location by the LS technique.

- Do linear interpolation/extrapolation or BEM with DPSS in time domain.

3) Interp:

- Estimate the channel response at each RS location by the LS technique.

- Do linear interpolation/extrapolation in frequency domain.

- Do linear interpolation/extrapolation in time domain.

4) KML and YML:

- Estimate the channel response at each RS location by the LS technique.

- Estimate the channel delay parameters by method K or Y on pilot symbols.

- Do LMMSE channel estimation in the frequency domain for pilot symbols.

- Do linear interpolation/extrapolation in time domain.

5) KD-MA, YD-MA, KL-MA, and YL-MA:

- Estimate the channel response at each RS location by the LS technique.

- Do linear interpolation/extrapolation or BEM with DPSS in time domain to create pseudo RR on all symbols.

- Estimate the channel delay parameters by method K or Y for all symbols.

- Do LMMSE channel estimation in the frequency domain on all symbols.

6) KDMD, YDMD, KDML, YDML, KLML, and YLML:

- Estimate the channel response at each RS location by the LS technique.

- Do linear interpolation/extrapolation or BEM with DPSS in time domain to create pseudo RR on pilot symbols.

- Estimate the channel delay parameters by method K or Y for pilot symbols.

- Do LMMSE channel estimation in the frequency domain on pilot symbols.

- Do linear interpolation/extrapolation or BEM with DPSS in time domain.

4.2.1 Validation with AWGN Channel

Before considering multipath channels, we first do simulation with an AWGN channel. Even though we usually do not encounter AWGN channels in practical wireless communication, it is a channel condition that facilitates easy theoretical analysis. We validate our methods and the simulation programs by examining the performance of MSE and SER curves resulting from simulation.

The theoretical MSE for linear frequency domain interpolation over the data symbols in AWGN can be found to be [14]

$$
\begin{aligned}
MSE &= \frac{1}{6} E[|\sum_{k=0}^{5} H_k - \hat{H}_k|^2] \\
&= \frac{1}{6} E[\sum_{k=0}^{5} |\{H_k - [\hat{H}_{k=0} + \frac{k}{6}(\hat{H}_{k=6} - \hat{H}_{k=0})]\}|^2] \\
&= \frac{1}{6} E[\sum_{k=0}^{5} |\{(\frac{k}{6})^2 + (\frac{6-k}{6})^2\}\sigma_W^2] \\
&= 0.676\sigma_W^2.
\end{aligned}
\tag{4.4}
$$

Where the relationship between σ_W^2 and SNR is given as

$$
\sigma_W^2 = \frac{1}{10^{SNR/10}}.
\tag{4.5}
$$

However, outside the outermost RS, no interpolation can be performed. So we do linear extrapolation on these subcarriers. The number of these data subcarriers will depend on the symbol location. When the number of data subcarriers outside the outermost RS is equal to
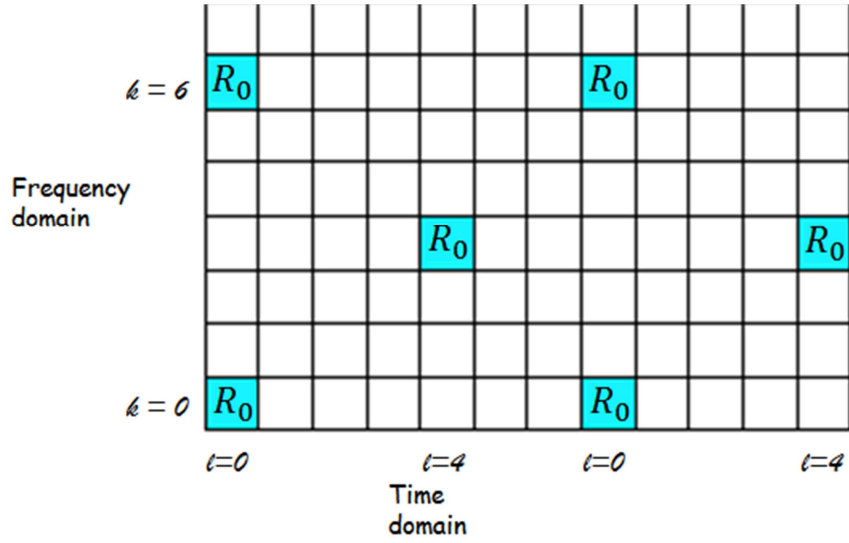
Figure 4.2: Different location of RS on different pilot symbols.

5, namely, the symbol index l in Figure 4.2 is equal to 0, the $MSE_{out=5,l=0}$ becomes

$$
\begin{aligned}
MSE_{out=5,l=0} &= \frac{1}{6}E[|\sum_{k=0}^{5} H_k - \hat{H}_k|^2] \\
&= \frac{1}{6}E[\sum_{k=0}^{5} |\{(\frac{k}{6})^2 + (\frac{6+k}{6})^2\}\sigma_W^2] \\
&= 2.34\sigma_W^2,
\end{aligned}
\tag{4.6}
$$

where subscript $()_{out}$ denotes the number of data subcarriers outside the outermost RS.

When the symbol index l is equal to 4, the number of data subcarriers outside the outermost RS in head and tail are 3 and 2, respectively. The $MSE_{out=3,l=4}$ and $MSE_{out=2,l=4}$ are $1.92\sigma_W^2$ and $1.639\sigma_W^2$, respectively. The theoretical MSE for linear FD interpolation over a pilot symbol in AWGN when $l = 0$ can be found as

$$
\begin{aligned}
MSE_{l=0} &= \frac{48 \cdot 0.676 + 2.34 * 2}{50}\sigma_W^2 \\
&= 0.74\sigma_W^2.
\end{aligned}
\tag{4.7}
$$

Similary, $MSE_{l=4}$ is $0.715\sigma_W^2$. The theoretical MSE for linear time domain interpolation over

44

the data symbols in AWGN can be found as

$$
\begin{aligned}
MSE &= \frac{1}{7}E[|\sum_{l=0}^{6} H_l - \hat{H}_l|^2] \\
&= \frac{1}{7}\left[E[\sum_{l=0}^{3}|\{H_l - [H_{RS,l=0} + \frac{l}{4}(H_{RS,l=0} - H_{RS,l=4})]\}|^2]\right] \\
&\quad + \frac{1}{7}\left[E[\sum_{l=4}^{6}|\{H_l - [H_{RS,l=4} + \frac{l}{3}(H_{RS,l=4} - H_{RS,l=7})]\}|^2]\right] \\
&= \frac{1}{7}\left[E[\sum_{l=0}^{3}|\{(\frac{l}{4})^2 \cdot 0.715 + (\frac{4-l}{4})^2 \cdot 0.74\}\sigma_W^2|]\right] \\
&\quad + \frac{1}{7}\left[[\sum_{l=4}^{6}\{(\frac{l-4}{3})^2 \cdot 0.74 + (\frac{7-l}{3})^2 \cdot 0.715\}\sigma_W^2|]\right] \\
&= 0.505\sigma_W^2.
\end{aligned}
\tag{4.8}
$$

For the 5-MHz case where the FFT size is 512 points, the theoretical MSE with linear frequency-domain interpolation over the whole band is therefore given by

$$
\begin{aligned}
MSE &= \frac{49 \cdot 0.505 + 0.74}{50}\sigma_W^2 \\
&= 0.510\sigma_W^2.
\end{aligned}
\tag{4.9}
$$

From Figure 4.3, we see that the MSE for "Interp" is equal to $0.513\sigma_W^2$. There is only 0.5% difference between the theoretical MSE and simulation the MSE. Furthermore, the theoretical MSE and the simulation MSE for "PerPL" are equal to $0.70051\sigma_W^2$ and $0.70055\sigma_W^2$, respectively, which are almost the same.

The theoretical MSE for "PerPD" is calculated as [12]

$$
MSE = bias^2 + var,
\tag{4.10}
$$

where var is given by [12]

$$
var \approx \sigma_W^2 \frac{D}{J},
\tag{4.11}
$$

with D and J being the number of the bases and number of pilot symbols, respectively. In Figure 4.3, $D = 5$ and $J = 15$. Hence $var_M \approx 0.33\sigma_W^2$ when SNR = 0 dB. Note that the value of $bias^2$ is about 10^{-7} according to simulation by setting noise equal to 0, namely, SNR= $+\infty$ dB ($\sigma_W^2 \longrightarrow 0$). Hence $bias^2$ is extremely small compared to noise for low SNR scenarios, and so we can neglect it when SNR is equal to 0 dB. We get

$$MSE = bias^2 + var \approx var \quad \text{for } var \gg bias^2. \tag{4.12}$$

The simulation MSE of "PerPD" is 0.316, it has 4% difference between simulation MSE and theoretical MSE.

The theoretical MSE by frequency domain LMMSE method will be reduced approximately by the filter order (i.e., filter tap numbers) times compared to only LS. It is given by [14]

$$MSE_{LMMSE} = \sigma_W^2 \frac{1}{S_L + \sigma_W^2}, \tag{4.13}$$

So the theoretical MSE with time domain interpolation is $0.7 \times \frac{1}{5}\sigma_W^2 = 0.14\sigma_W^2$. However, the simulation result is at about 25% difference for both "KML" and "YML" when SNR is equal to 0 dB. Such difference is caused by channel delay parameters estimation error, which causes high deviation on correlation matrix due to noise power is large compared to signal power. For the case where SNR is equal to 20 dB, the MSE values of theoretical LMMSE, "KML", and "YML" are $0.175\cdot10^{-3}$, $0.183\cdot10^{-3}$, and $0.192\cdot10^{-3}$, respectively. There are 5% and 10% differences between theoretical and simulation for "KML" and "YML," respectively. These differences are caused by different way of channel parameters computation, which introduces different errors in different environments.

The theoretical MSE of the other methods are not verified, because the component method, i.e., method K, method Y, BEM with DPSS and linear interpolation/extrapolation, are already validated by comparing theoretical MSE and simulation MSE. Since the other

methods are combinations of the validated component methods, we can trust the simulation results.

Note that the dimension of DPSS and time-bandwidth product are set to 7 and 2, respectively, if not noted in later simulation results.

4.2.2 Simulation Results for Multipath Channels

Figures 4.4–4.21 show the performance of different channel estimation methods at different velocities in different channels. Here we take Figure 4.12 for instance. When SNR = 0db and 20db, the MSE of "ALS" are 10^0 and 10^{-2}, respectively. The MSE of "ALS" is inversely proportional to SNR as we expected. We infer that this phenomenon is due to every subcarrier is RS, the only uncertainty is noise. Thus the MSE should inversely proportional to SNR when we only use the LS channel estimation method. The MSE of "PerPL" is higher then that of "PerPD" because linear interpolation is not a good method for high speed scenario, whereas BEM with DPSS is also outstanding in this condition. We can see that the error floor of "PerPD" is quiet lower then that of "PerPL". It conforms with we expected. The remaining methods without producing pseudo RR are "Interp", "KML" and "YML", the performance of which are quiet worse in this situation. The MSE of these methods reach error floor very soon because the RMS delay spread of SUI-5 is relatively large, thus the coherence bandwidth is smaller then the distance of adjacent RSs. The remaining methods are associated with producing pseudo RR, however, the performance of which can vary dramatically with different methods. Here we take "YDMD", "YDML" and "YLML" for example. The MSE of "YDMD" is good in this condition, and the MSE of "YDML" is similar to that of "YDMD". However, "YLML" is not a good choice in this environment. The performance of "YLML" is better then that of methods without producing pseudo RR, but is the worst choice in methods with producing pseudo RR. The reason of this phenomenon comes from

47

linear interpolation. Producing pseudo RR via linear interpolation in high speed scenario make the pseudo RR quiet different to the actual channel response. The bad performance is due to we treat these pseudo RR as original channel response at RS subcarriers.

By observing Figures 4.4–4.21, we can get some initial conclusions. The performance of "YL-MA" is similar to that of "YLML"; the same feature is discovered in groups {KL-MA, KLML}, {YDMD, YDML, YD-MA}, and {KDMD, KDML, KD-MA}. We infer that this phenomenon is due to the first two steps, that is to say, the method for creating pseudo RR and the method for estimating channel delay parameters. The methods subsequent to first two have little difference in simulation result, but we can still find that linear interpolation is a worst choice when the moving speed increases. For the following discussion, we label each group according to first two letters as follows.

YD) :

- YD-MA

- YDMD

- YDML

KD) :

- KD-MA

- KDMD

- KDML

YL) :

- YL-MA
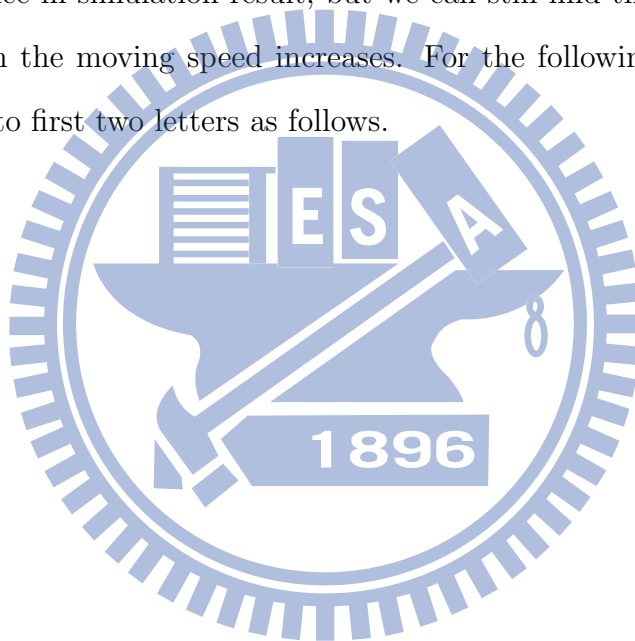
- YLML

KL) :

- KL-MA

- KLML

Low SNR, low to moderate speed environment, high τ_{rms}

The KL group performs better than the KD group in this situation. The distance between adjacent pilots in time domain is equal to 7 symbols, where the linear interpolation method reduces the noise variance in the LS estimation from σ_W^2 to $0.71\sigma_W^2$ for each RB and the BEM with DPSS method reduces it from σ_W^2 to $0.9375\sigma_W^2$ approximately by (4.11). Recall that $bias^2$ can be ignored in this situation. The YL group performs better than the YD group in this scenario as well. The reason of this phenomenon is the same as that between KL and KD. Methods "KML" and "YML" are worse at higher τ_{rms}; the main reason is that they do not use pseudo RR.

High SNR, low to moderate speed environment, high τ_{rms}

Methods "KML" and "YML" perform worse as higher τ_{rms}; the reason is the same as in the previous situation. The result of the KD group is better than that of the KL group at higher speeds. Noise is not an important issue in this condition. We can see the BEM with DPSS method outperforms the linear interpolation. The YD group and the YL group also follow this relationship.

Low to high SNR, high speed environment, high τ_{rms}

Every method performs worse in this condition. But the KL group performs better than the KD group when the SNR is low. However, the KL group reaches error floor very soon.

The problem is mainly caused by linear interpolation. When the moving speed is high, the pseudo RR estimated by linear interpolation is far from the actual signal. Thus the performance get worse if we treat pseudo RR as original channel response at RS subcarriers. Their error floor may be higher than just doing liner interpolation in both time domain and frequency domain in some cases. The YD group and the YL group also follow this relationship. Methods "KML" and "YML" are not good under this condition.

Low to high SNR, low to high speed environment, low τ_{rms} (SUI-2)

Consider the SUI2 channel. The τ_{rms} here is small; in other words, the coherence bandwidth is large. The KD group and the YD group are still good in SUI-2, and we can see that their performance is close to that of "YML" and "KML." The YL group and the KL group perform better than the KD group and the YD group in low SNR scenario. However, both groups degrade dramatically than other methods as the moving speed increases. This is due to pseudo RR are generated by linear interpolation, which is not suitable at the condition of high moving speeds.

Channel with more taps

The results for channels having mora than three taps in their PDPs are shown in Figures 4.13–4.21. The performance of the YD group and the KD group is good. The methods without using pseudo RR are good at TU and VA models at low to moderate speed environment. But as in the case of the SUI channels, the methods without using pseudo RR get worse as the moving speed increases. We thus have shown by simulations that using pseudo RR can benefit the channel estimation performance, as it is intuitively expected.

Performance difference between with and without tap adjustment

The results are shown in Figures 4.20–4.23. We can find that the performance between with and without tap adjustment are almost the same in Figure 4.20 and Figure 4.22 when the moving speed is equal to 120 km/h. The same circumstance is also shown in 300km/h scenario by examining Figure 4.21 and Figure 4.23. Thus we think that tap adjustment can be employed with little difference for saving memories issue.
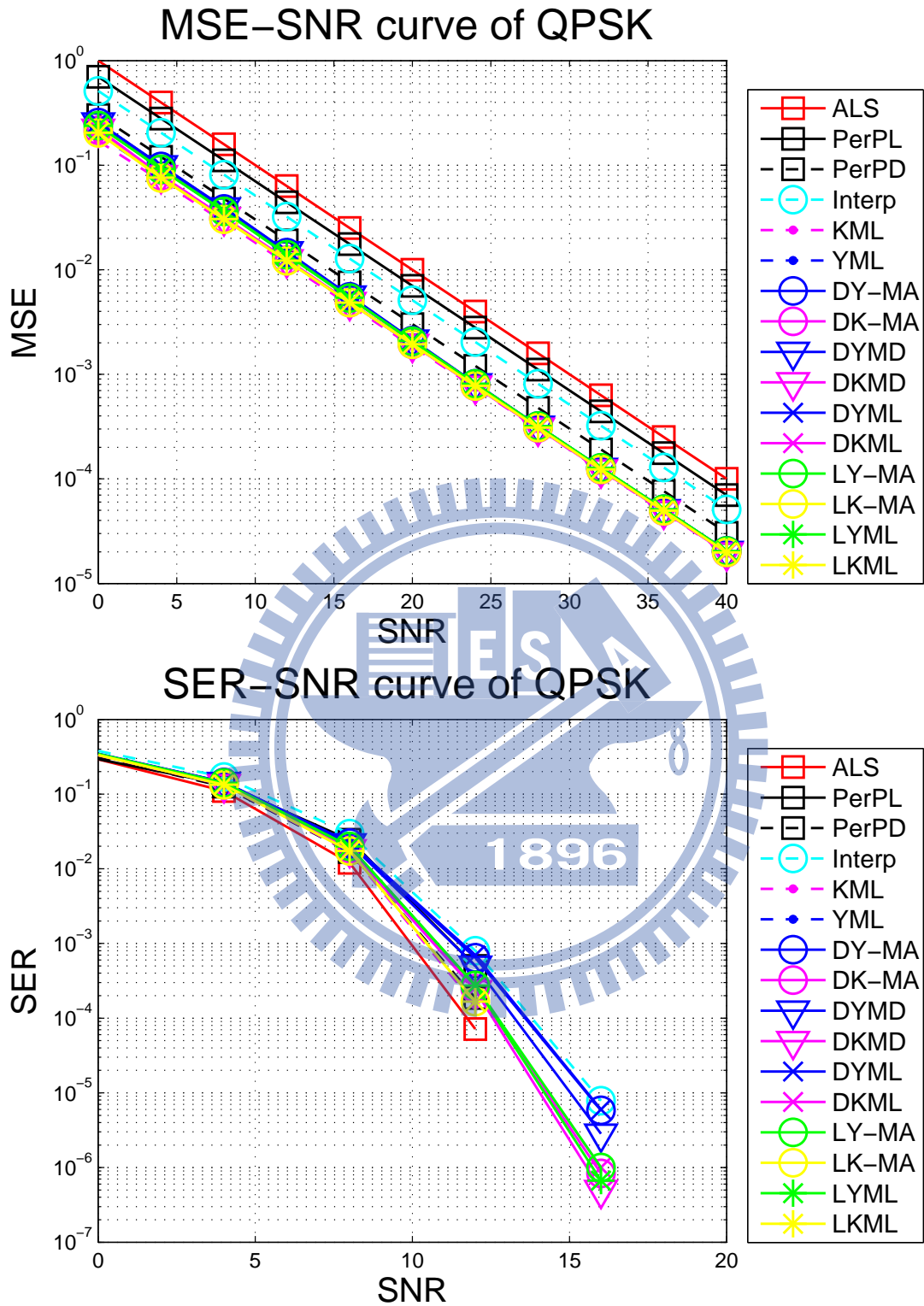
Figure 4.3: Channel estimation MSE and SER for QPSK in AWGN channel for LTE downlink with FFT size = 512, dimension of DPSS = 5, and time-bandwidth product = 1.
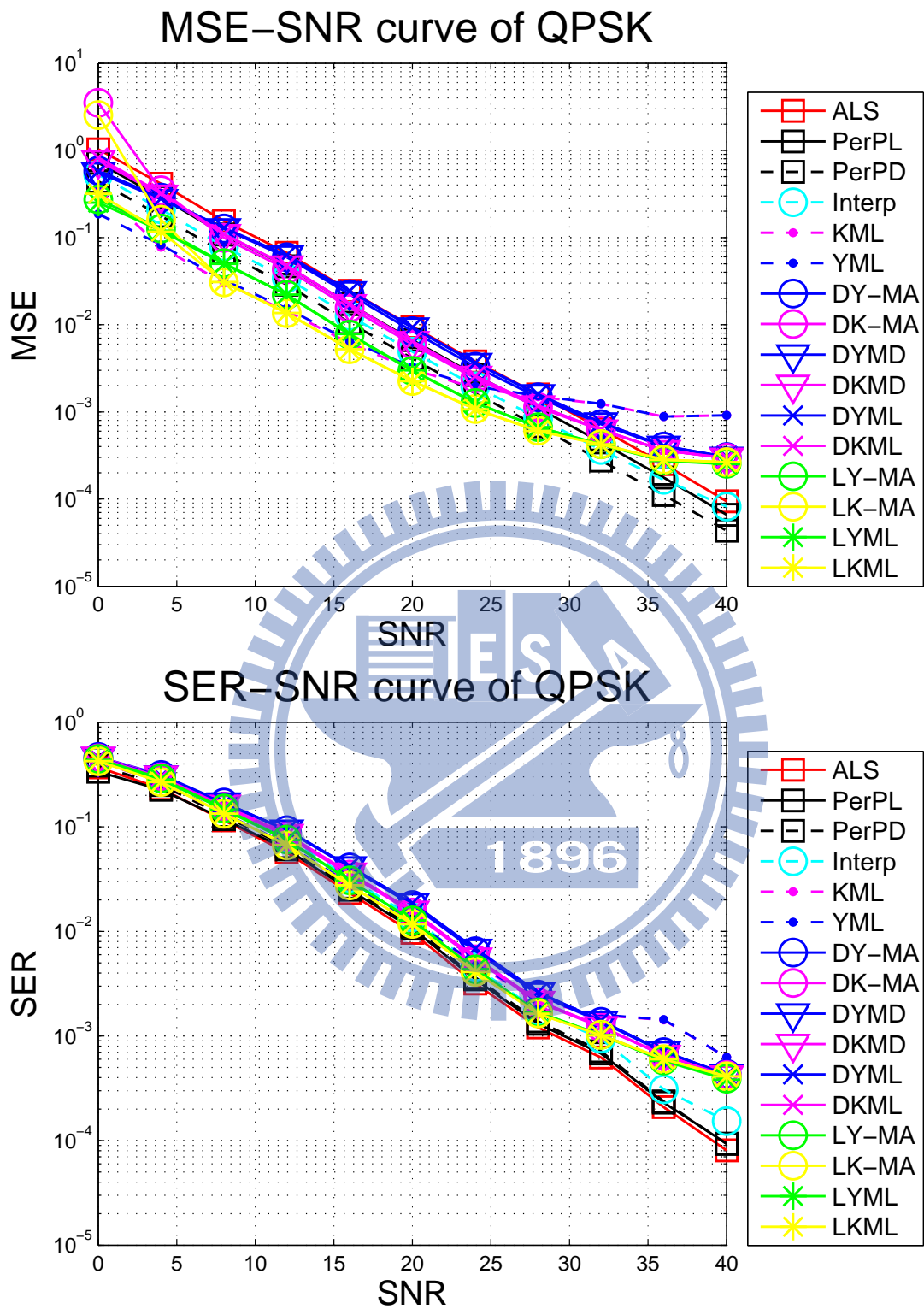
Figure 4.4: Channel estimation MSE and SER for QPSK in SUI2 channel for LTE downlink with FFT size = 512, and moving speed = 3 km/h.
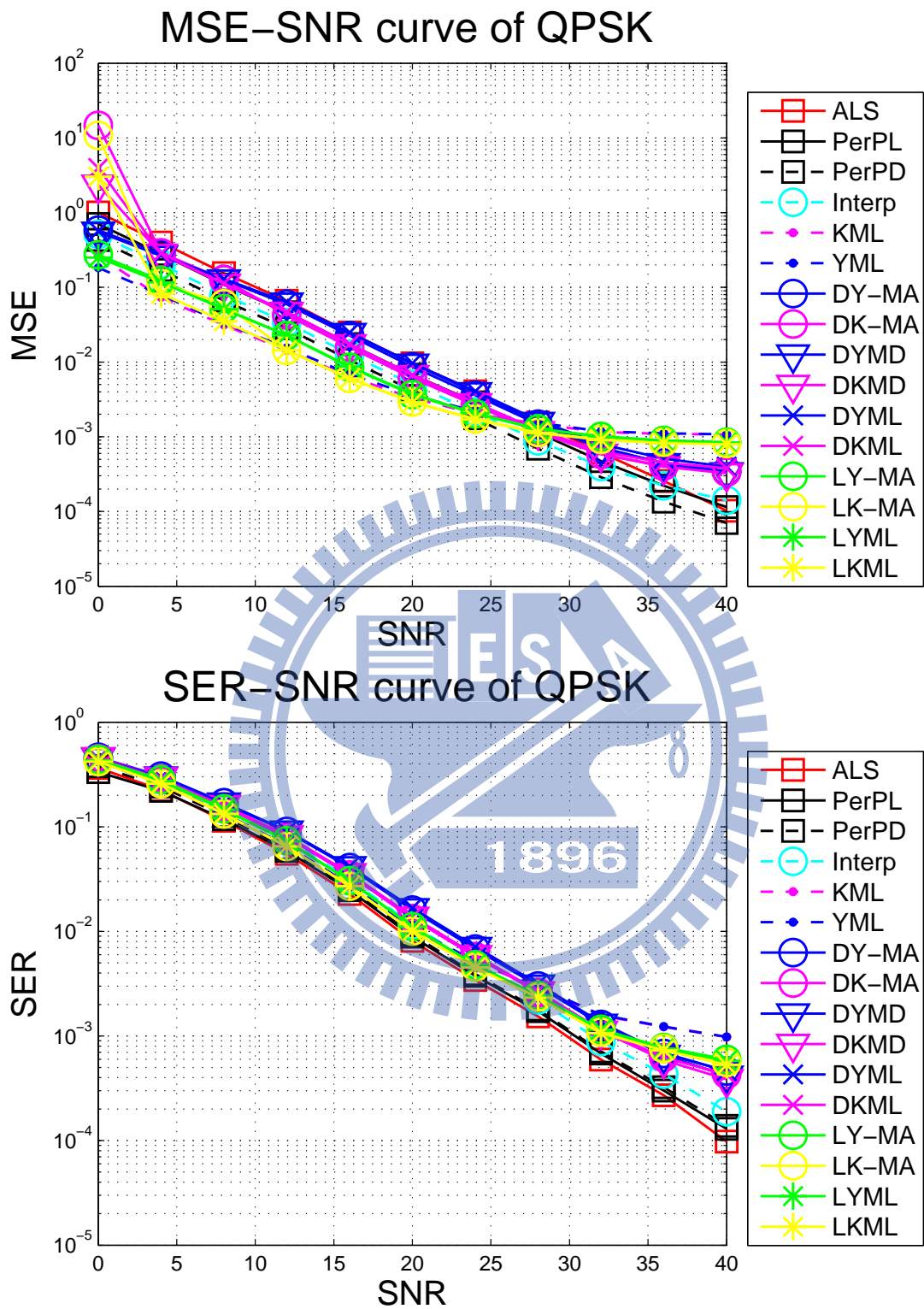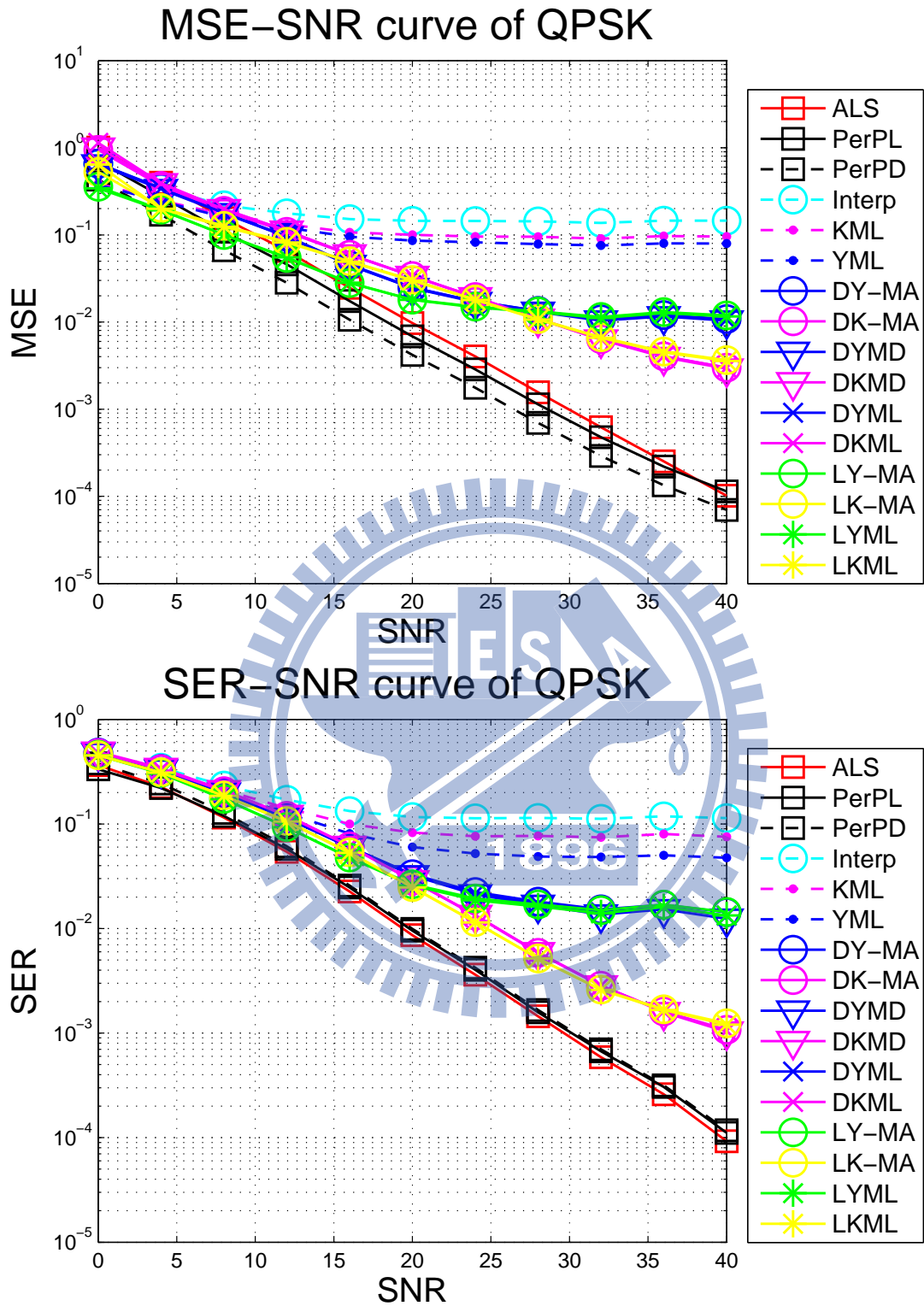
Figure 4.5: Channel estimation MSE and SER for QPSK in SUI2 channel for LTE downlink with FFT size = 512, and moving speed = 120 km/h.
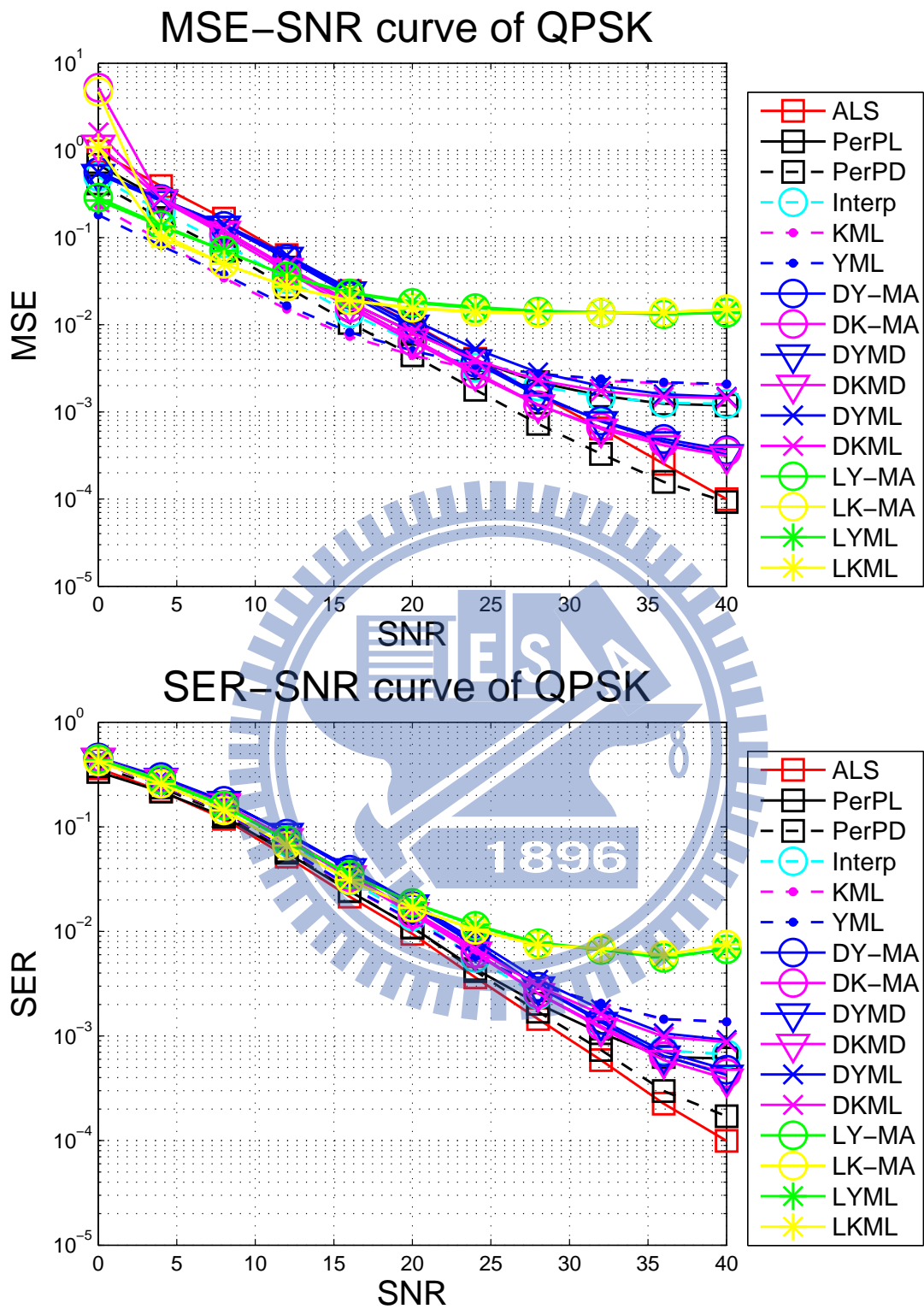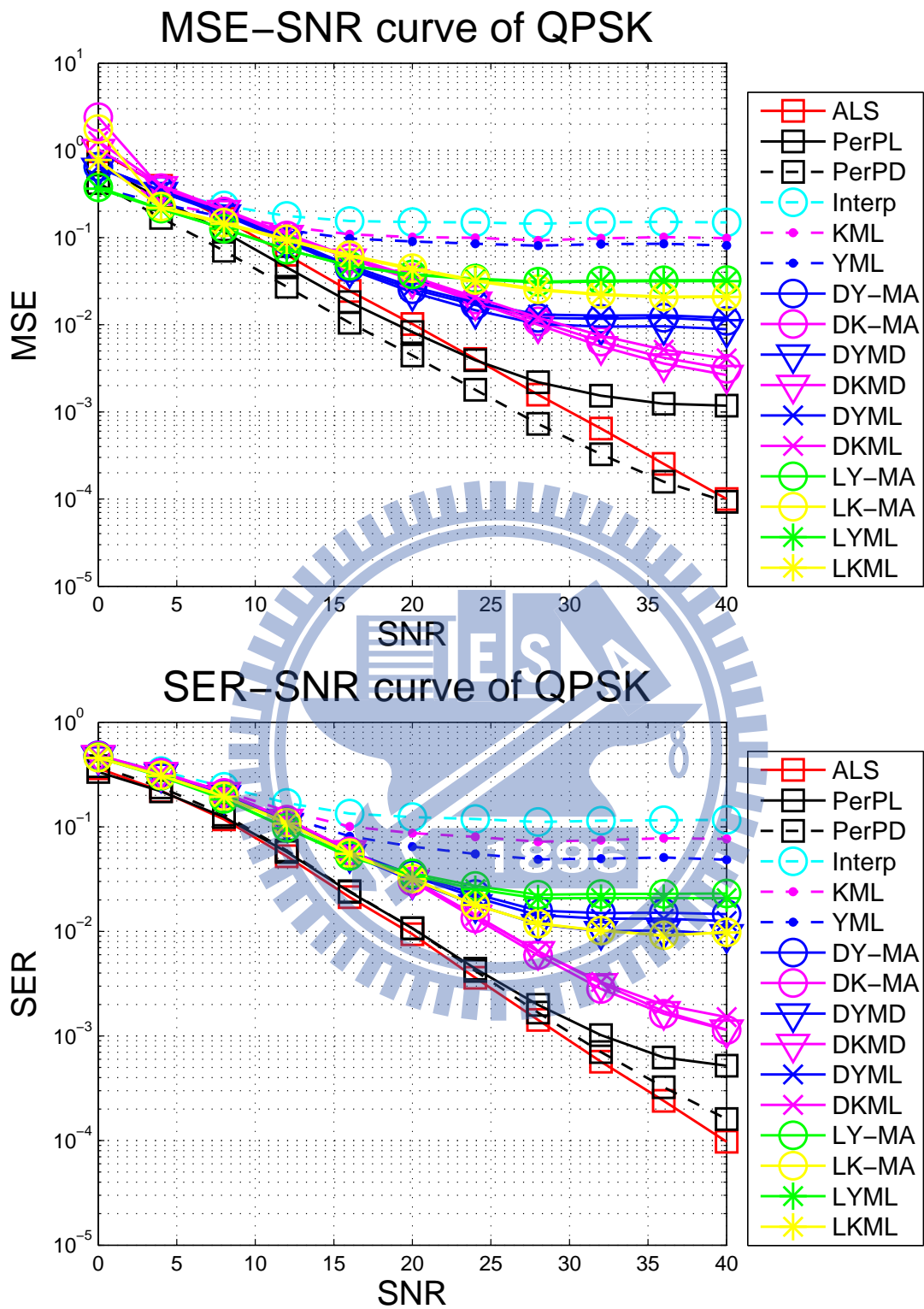
Figure 4.6: Channel estimation MSE and SER for QPSK in SUI2 channel for LTE downlink with FFT size = 512, and moving speed = 300 km/h.
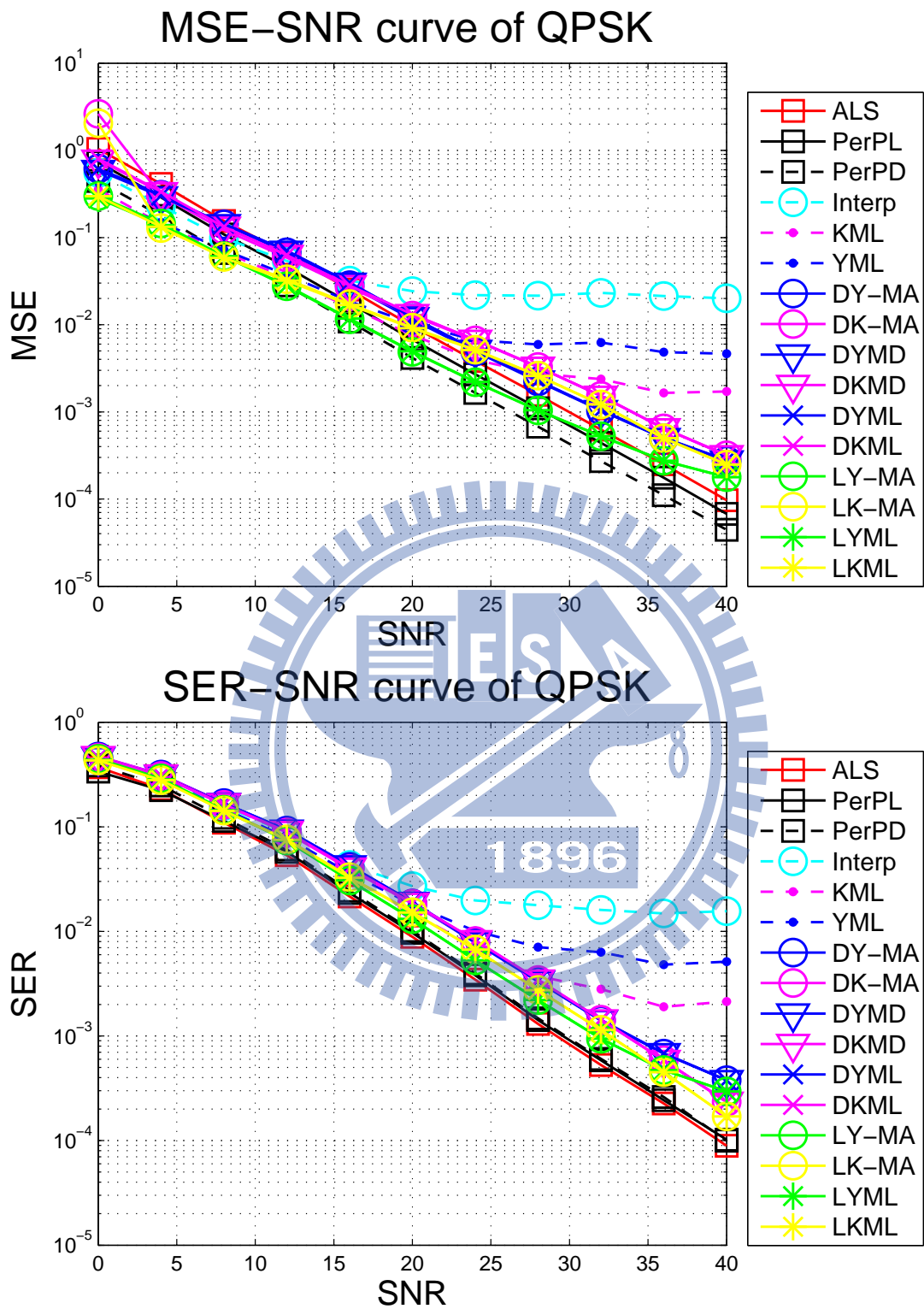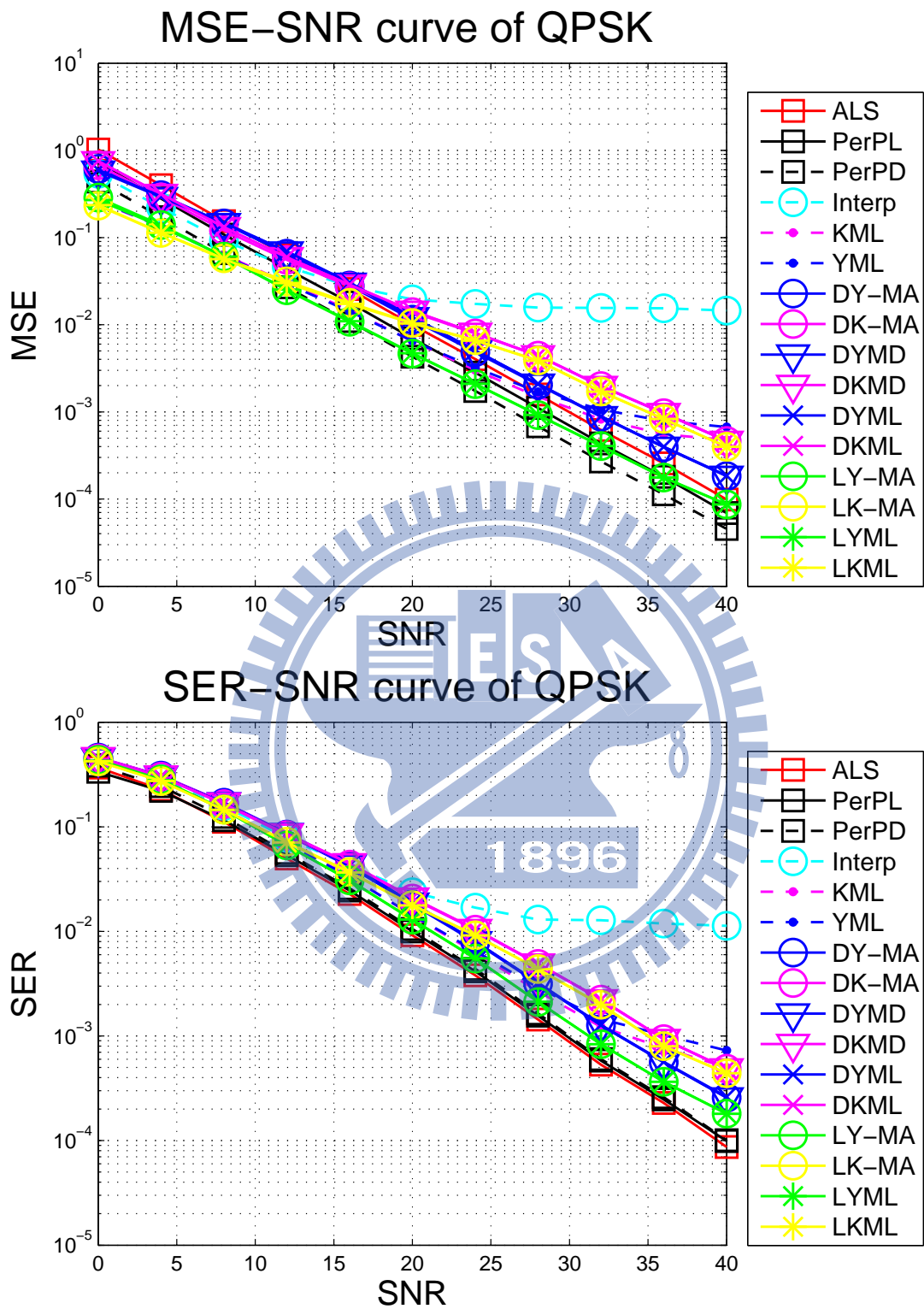
Figure 4.7: Channel estimation MSE and SER for QPSK in SUI4 channel for LTE downlink with FFT size = 512, and moving speed = 3 km/h.
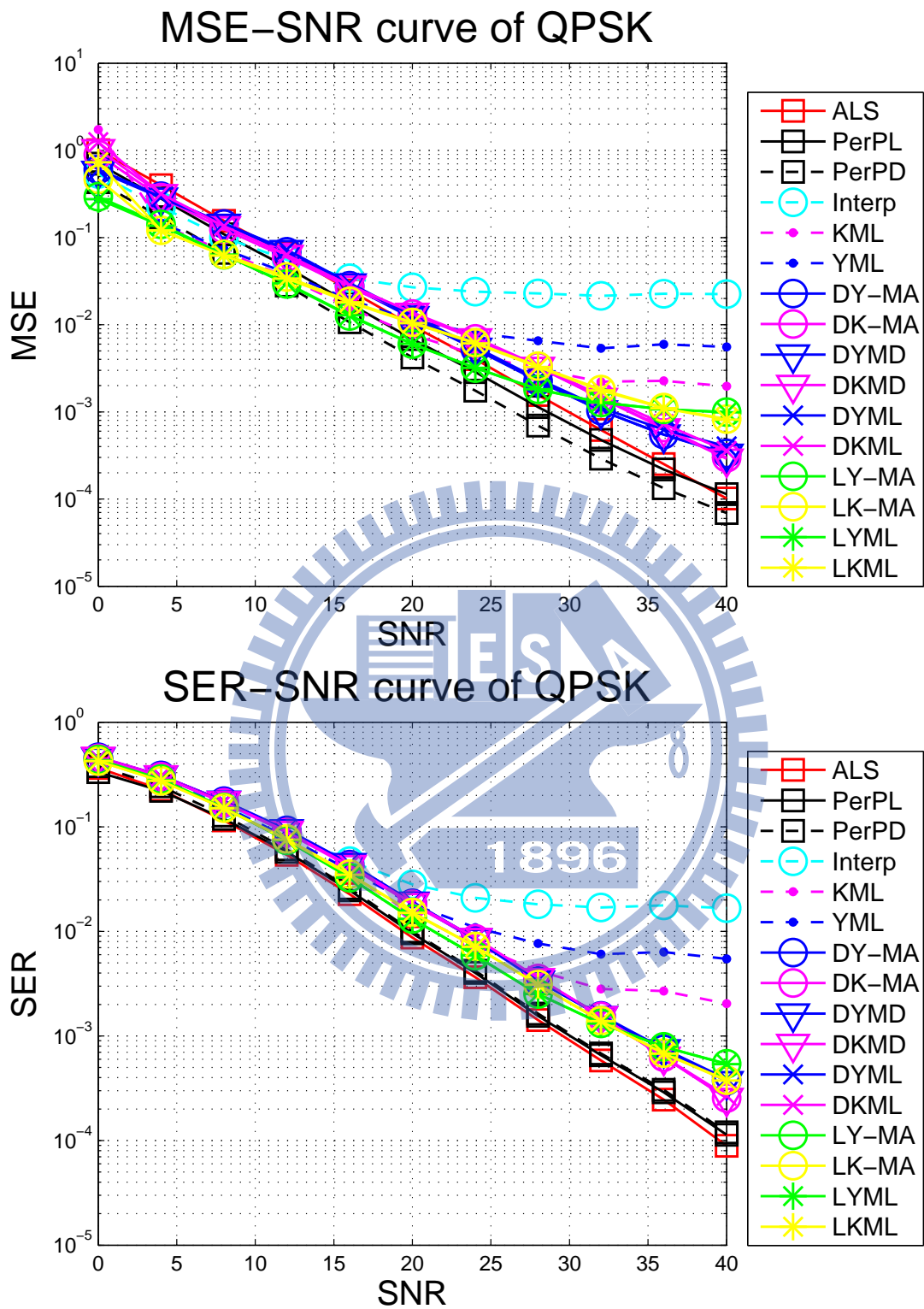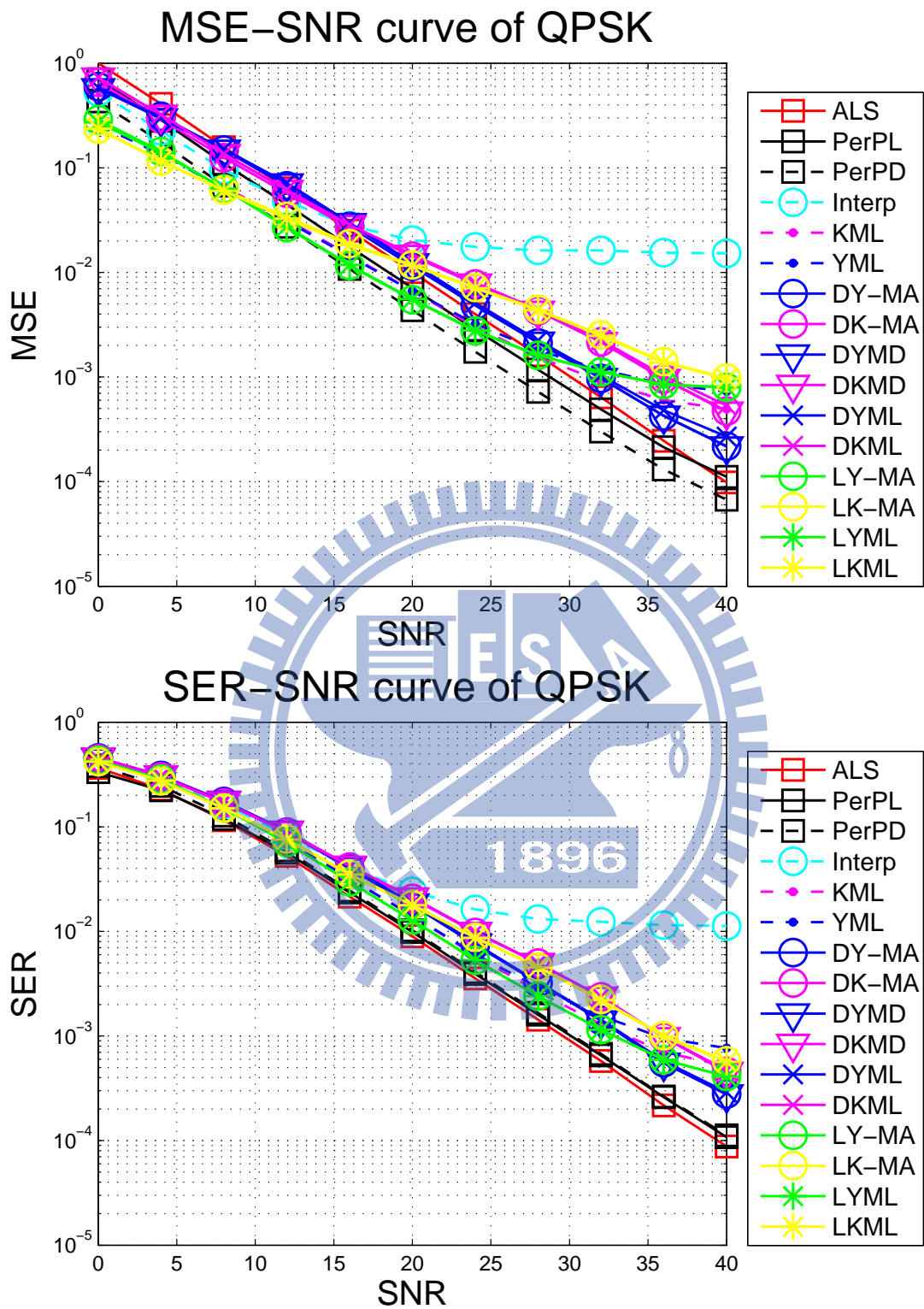
Figure 4.8: Channel estimation MSE and SER for QPSK in SUI4 channel for LTE downlink with FFT size = 512, and moving speed = 120 km/h.
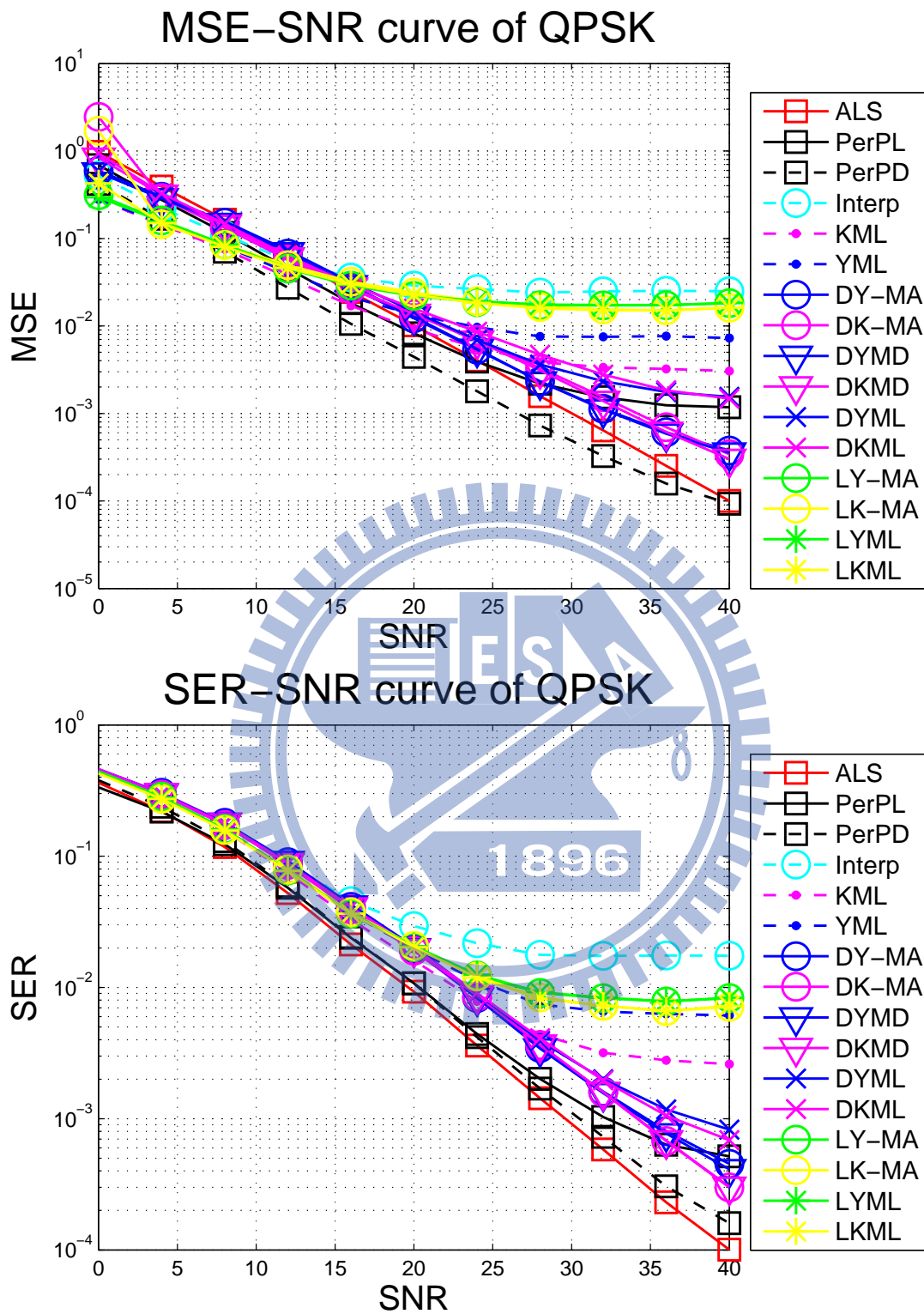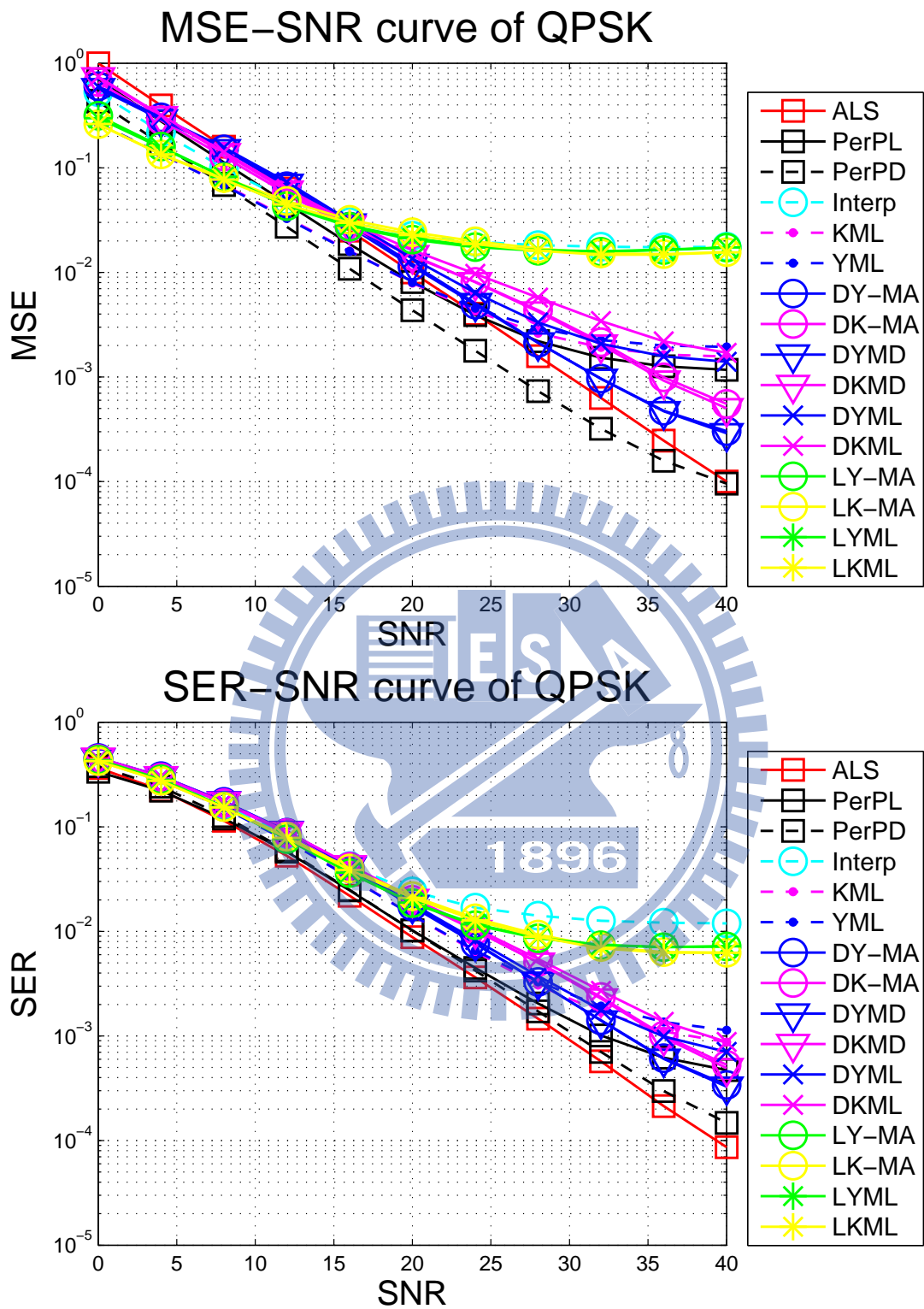
Figure 4.9: Channel estimation MSE and SER for QPSK in SUI4 channel for LTE downlink with FFT size = 512, and moving speed = 300 km/h.
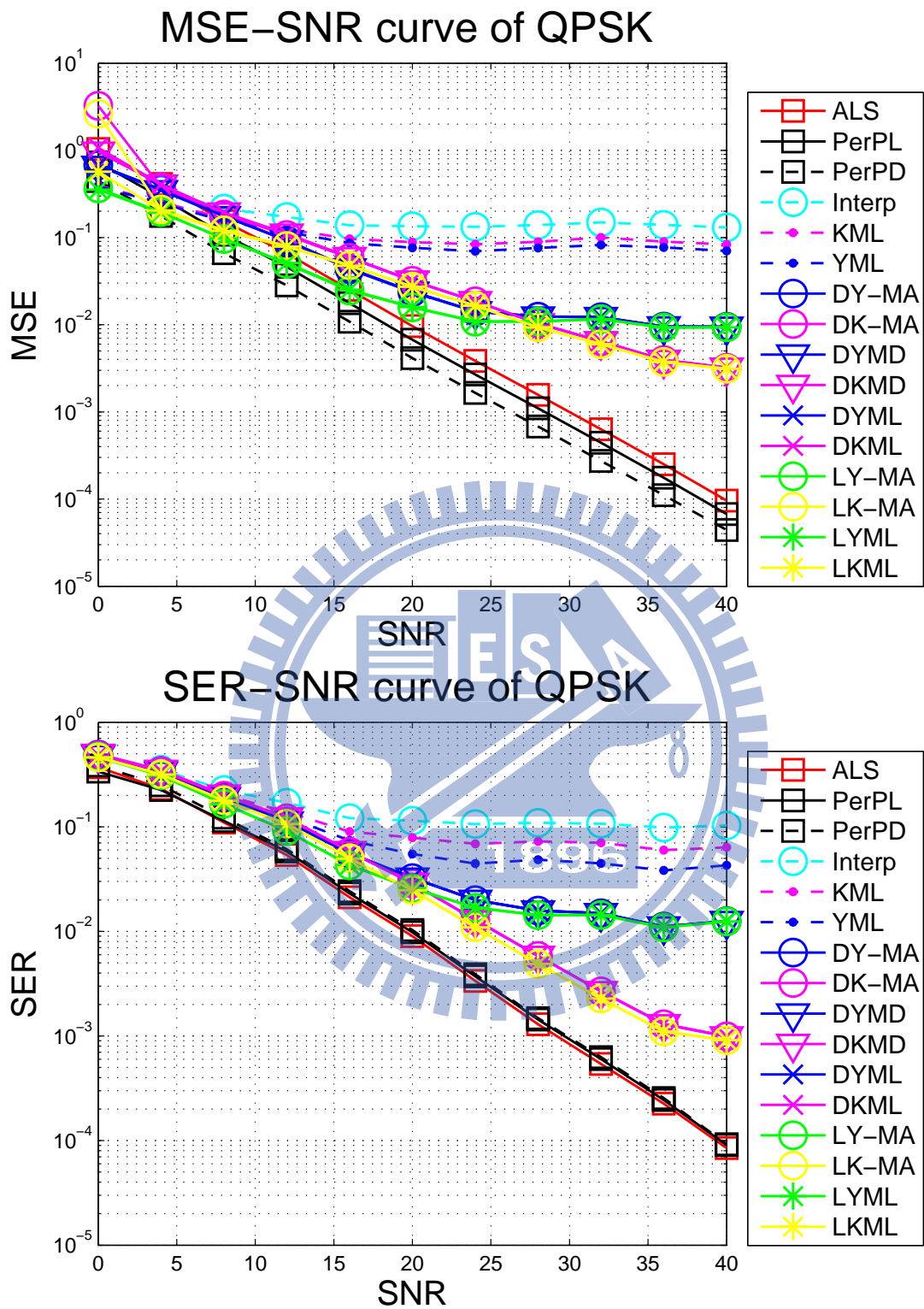
Figure 4.10: Channel estimation MSE and SER for QPSK in SUI5 channel for LTE downlink with FFT size = 512, and moving speed = 3 km/h.

Figure 4.11: Channel estimation MSE and SER for QPSK in SUI5 channel for LTE downlink with FFT size = 512, and moving speed = 120 km/h.

Figure 4.12: Channel estimation MSE and SER for QPSK in SUI5 channel for LTE downlink with FFT size = 512, and moving speed = 300 km/h.
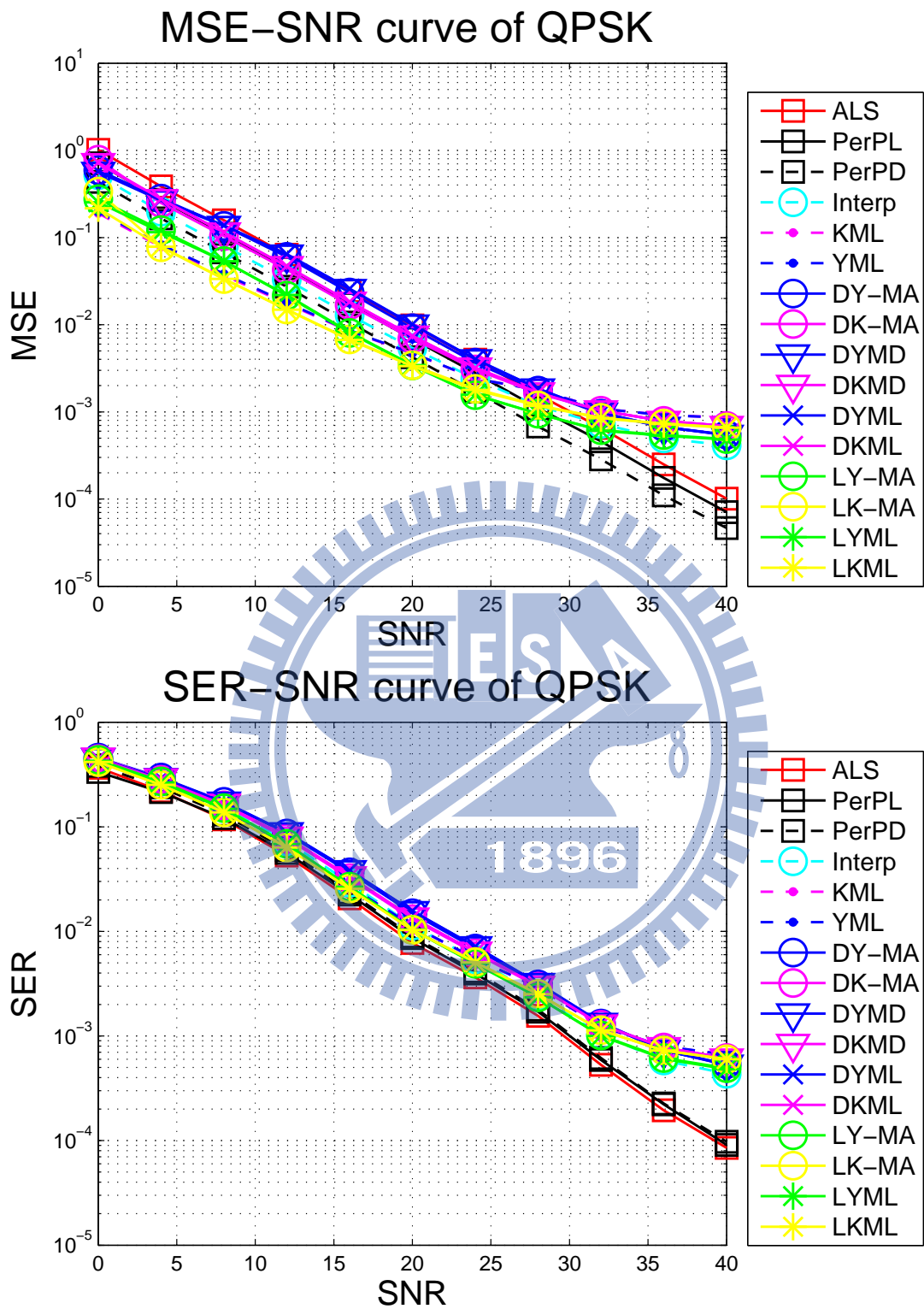
Figure 4.13: Channel estimation MSE and SER for QPSK in TU channel for LTE downlink with FFT size = 512, and moving speed = 3 km/h.
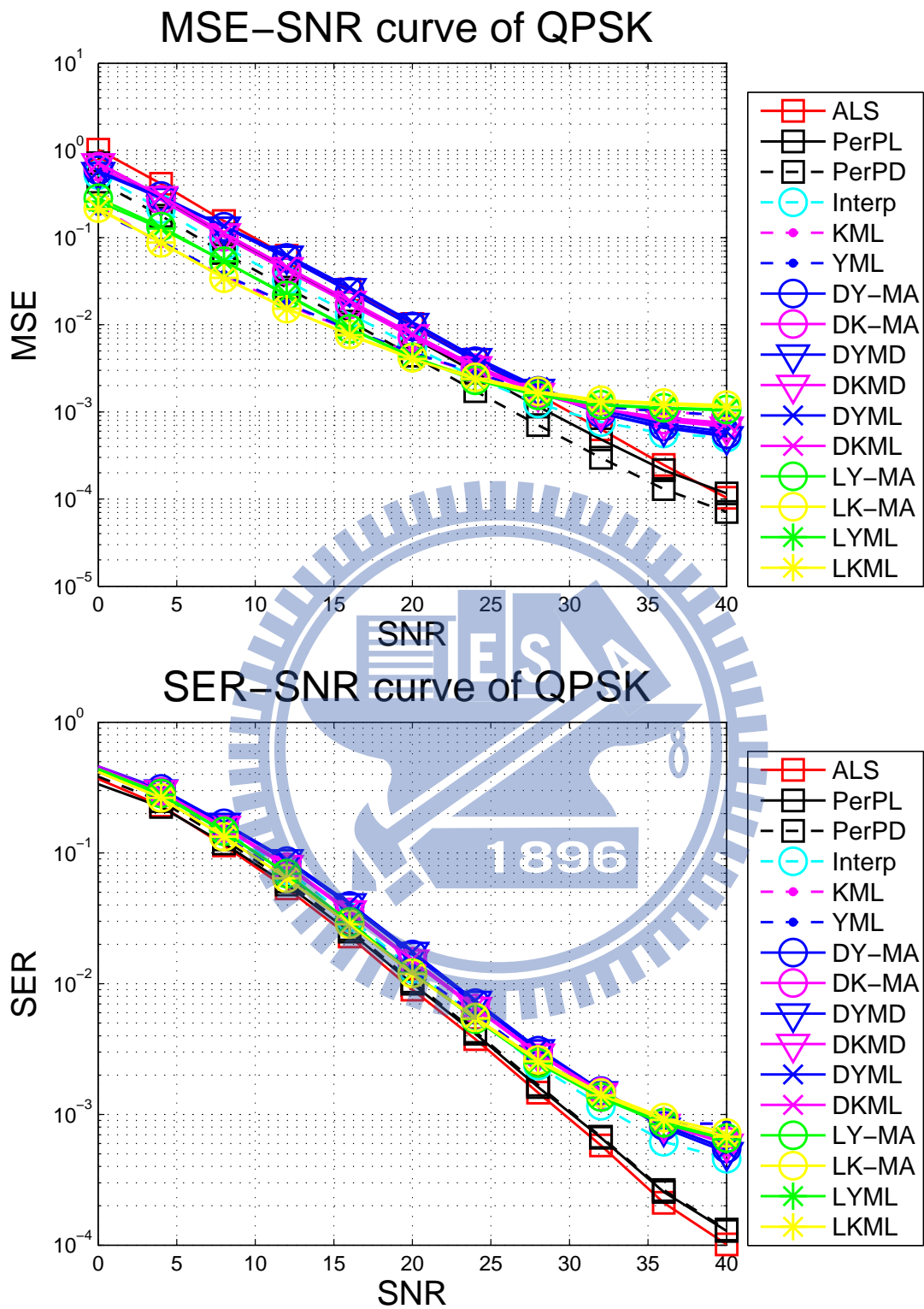
Figure 4.14: Channel estimation MSE and SER for QPSK in TU channel for LTE downlink with FFT size = 512, and moving speed = 120 km/h.

63

Figure 4.15: Channel estimation MSE and SER for QPSK in TU channel for LTE downlink with FFT size = 512, and moving speed = 300 km/h.
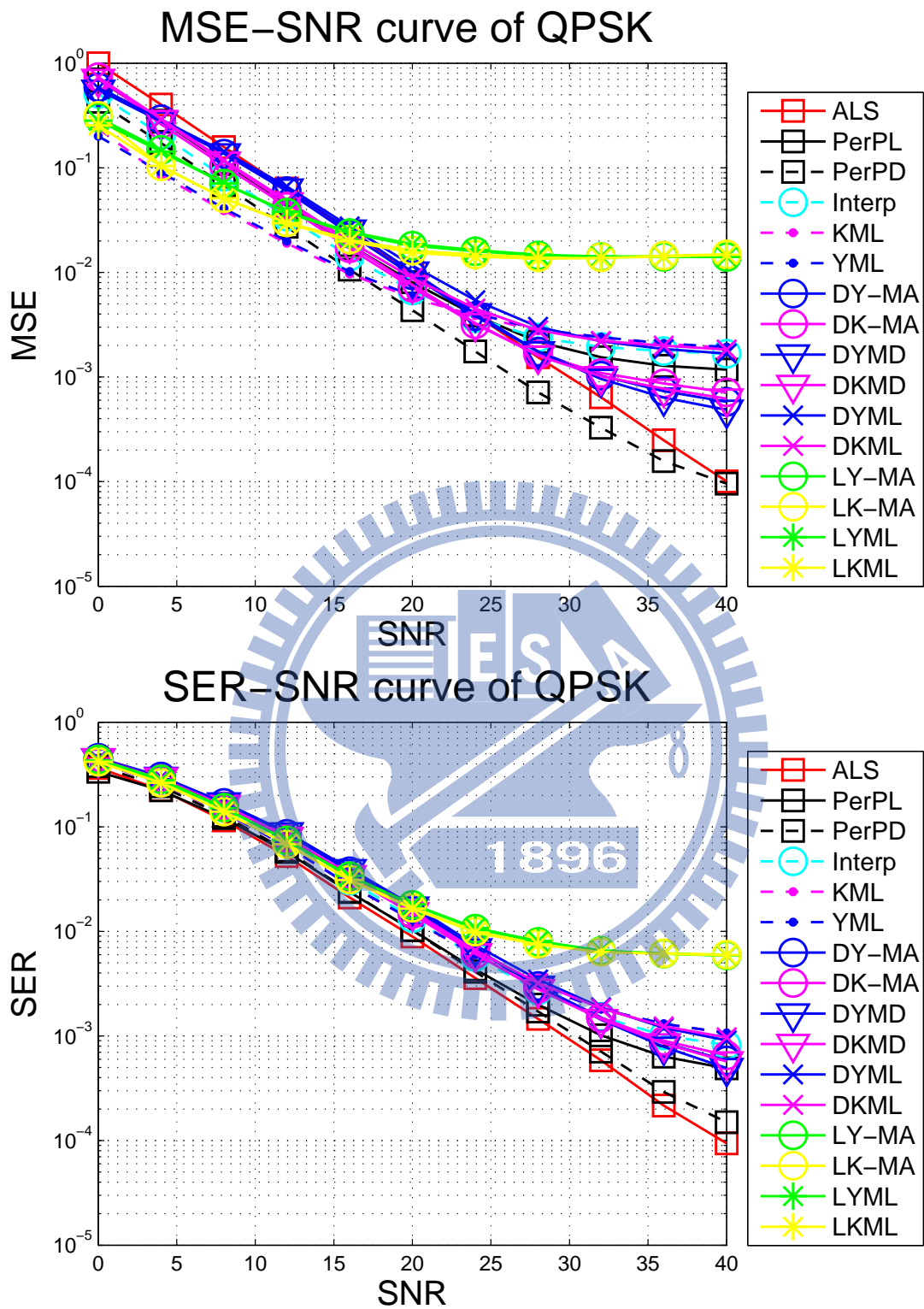
Figure 4.16: Channel estimation MSE and SER for QPSK in ITU-VA channel for LTE downlink with FFT size = 512, and moving speed = 3 km/h.

Figure 4.17: Channel estimation MSE and SER for QPSK in ITU-VA channel for LTE downlink with FFT size = 512, and moving speed = 120 km/h.

Figure 4.18: Channel estimation MSE and SER for QPSK in ITU-VA channel for LTE downlink with FFT size = 512, and moving speed = 300 km/h.
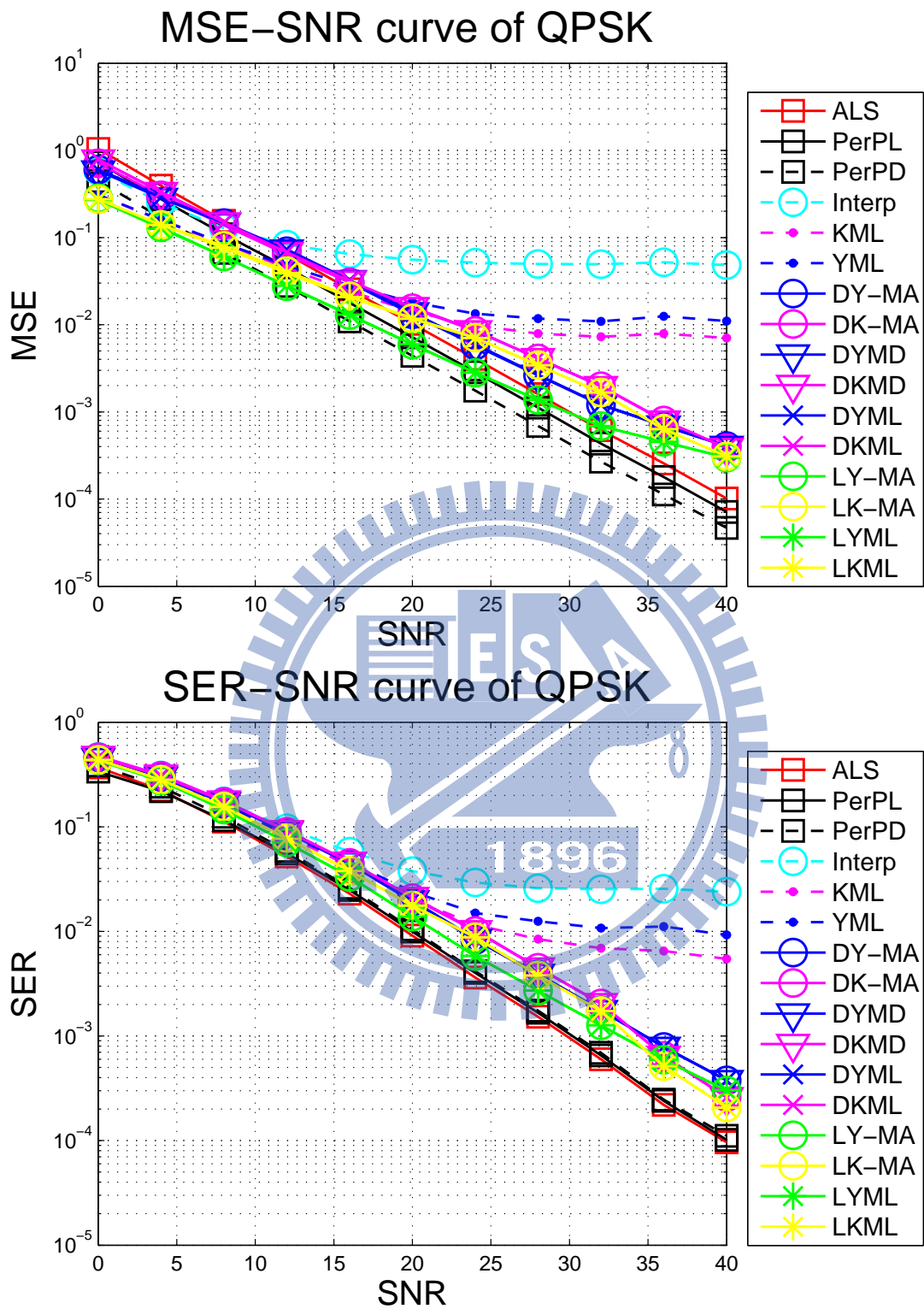
Figure 4.19: Channel estimation MSE and SER for QPSK in artificial ITU-VA channel for LTE downlink with FFT size = 512, and moving speed = 3 km/h.
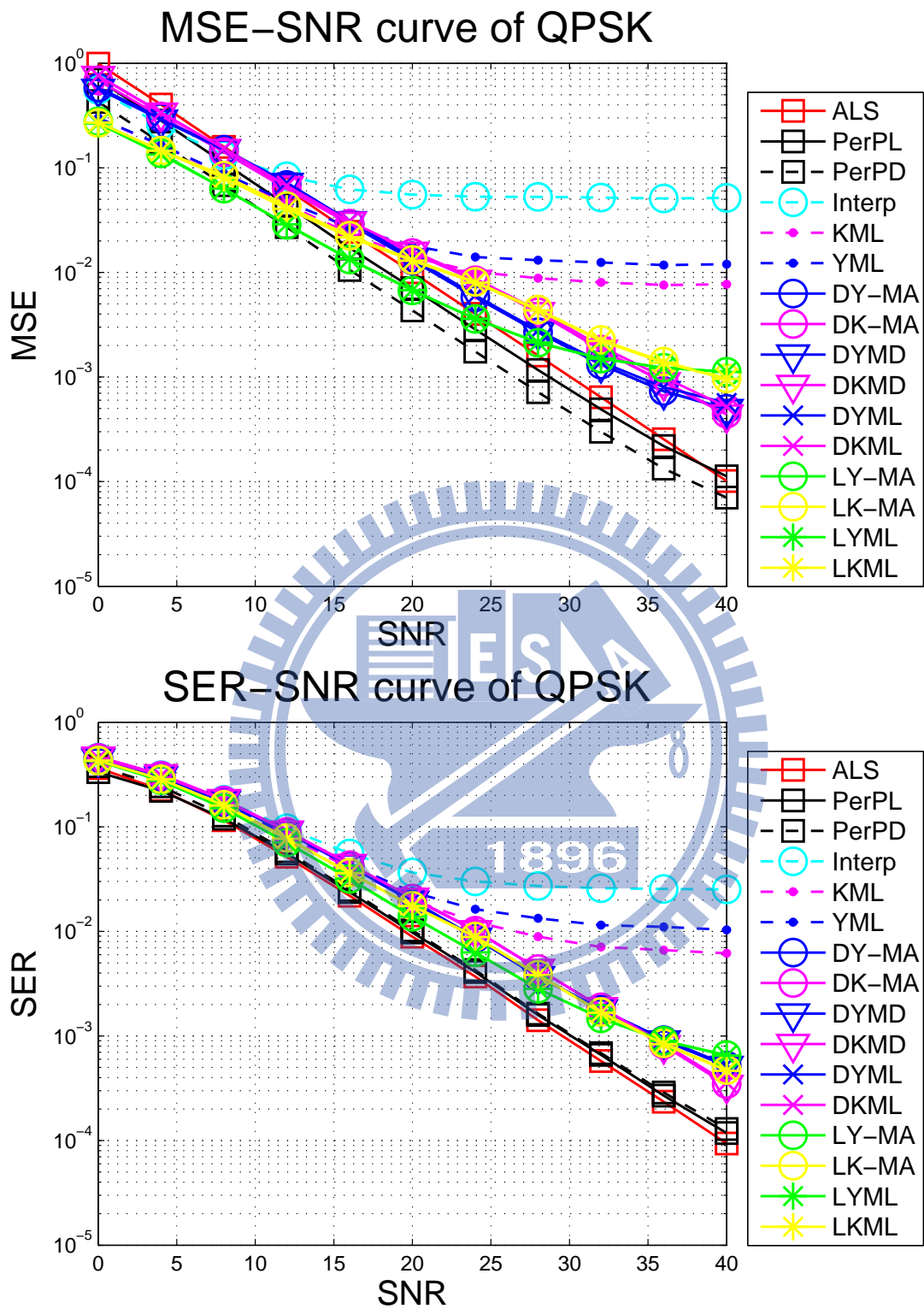
Figure 4.20: Channel estimation MSE and SER for QPSK in artificial ITU-VA channel for LTE downlink with FFT size = 512, and moving speed = 120 km/h.
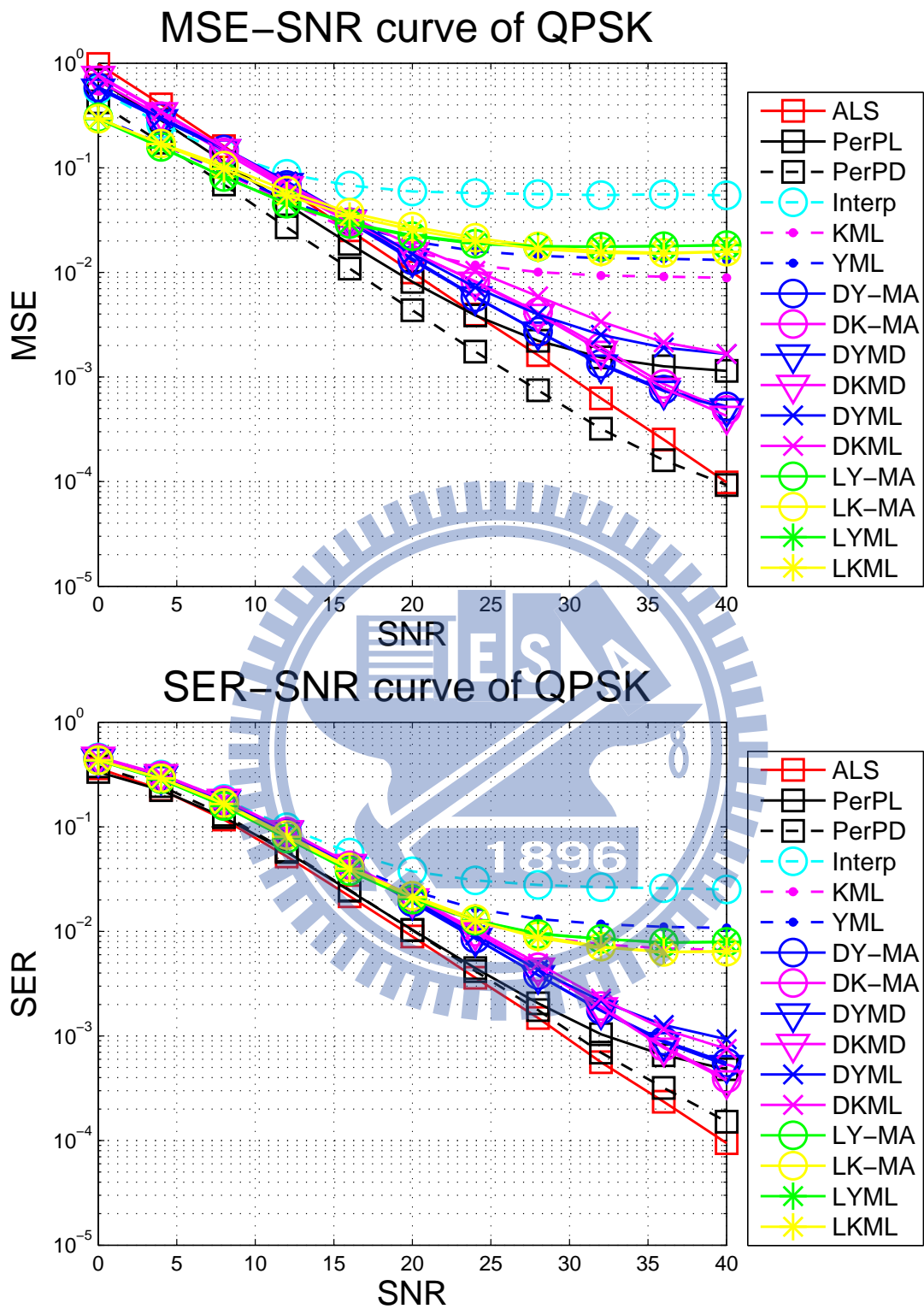
Figure 4.21: Channel estimation MSE and SER for QPSK in artificial ITU-VA channel for LTE downlink with FFT size = 512, and moving speed = 300 km/h.

Figure 4.22: Channel estimation MSE and SER for QPSK in artificial ITU-VA channel for LTE downlink with FFT size = 512, moving speed = 120 km/h, and without tap adjustment.
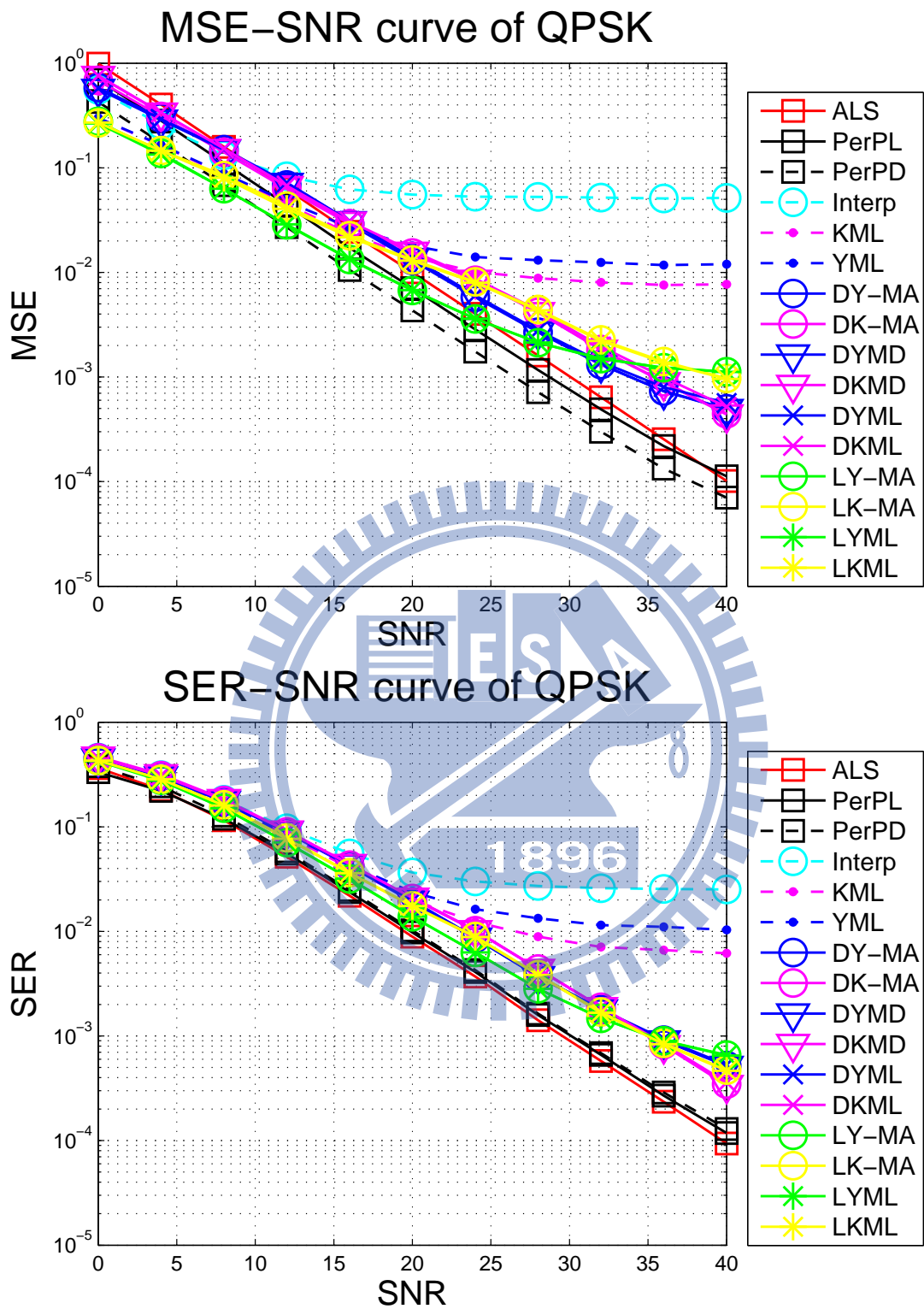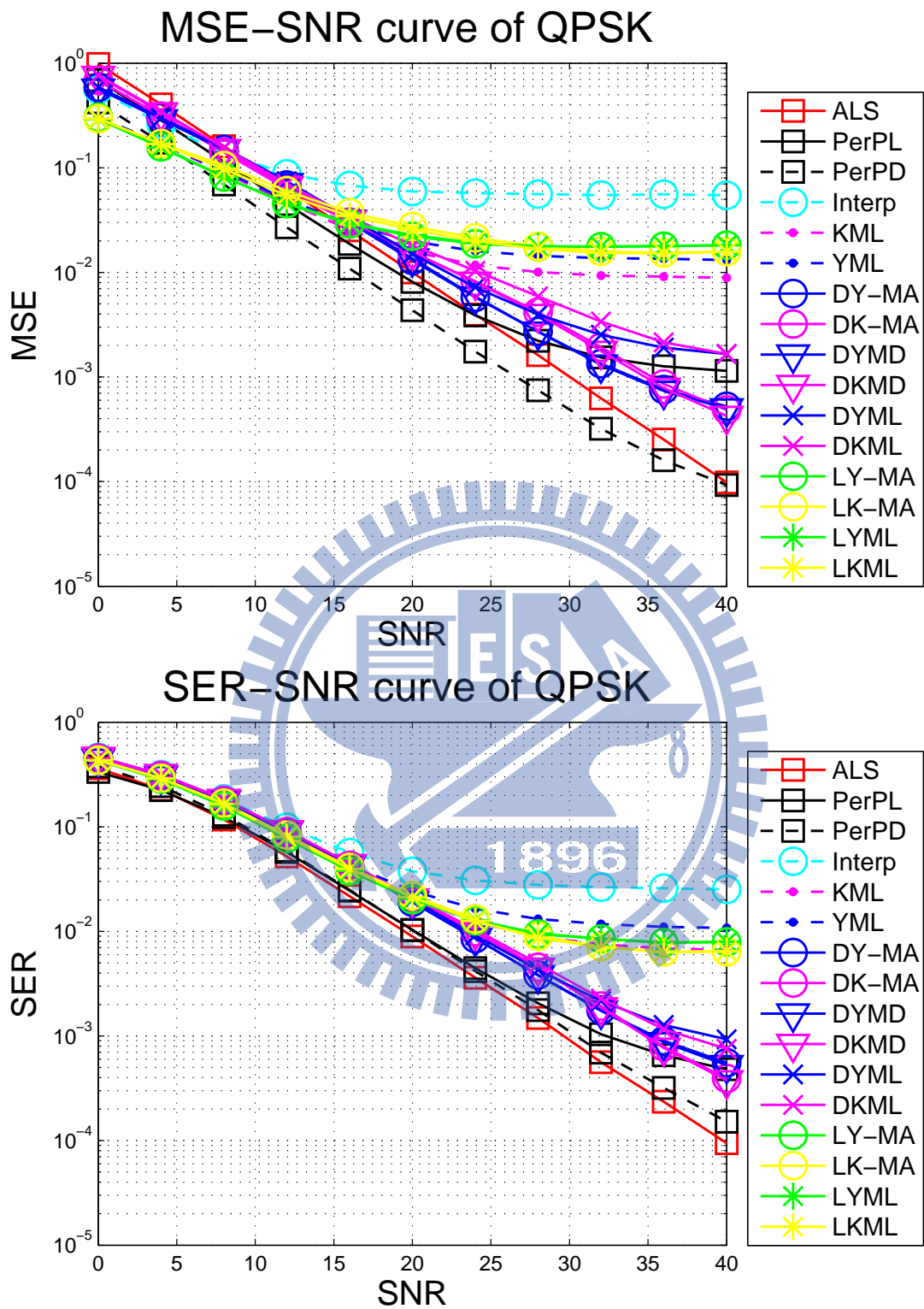
Figure 4.23: Channel estimation MSE and SER for QPSK in artificial ITU-VA channel for LTE downlink with FFT size = 512, moving speed = 300 km/h, and without tap adjustment.

Chapter 5

Conclusion and Future Work

5.1 Conclusion

In chapter three, we presented several channel estimation methods, which are LS, LMMSE and BEM with DPSS, for OFDMA downlink for LTE and LTE-A PDSCH. Under the LTE DL system, we first do LS method in FD to get initial channel frequency response then we do LMMSE channel estimation. For the LMMSE channel estimator, there are two methods for getting autocorrelation function via estimating RMS delay spread and mean delay. To improve the accuracy of the estimated channel delay parameters, we combined with the idea of producing some pseudo RR by linear interpolation or use of BEM with DPSS in TD of channel response estimates at the RS subcarriers in some other pilot symbol then doing LMMSE channel estimation. Finally, we estimate remaining data signals via linear interpolation or use of BEM with DPSS in TD of channel response estimates at the data subcarriers in notpilot symbols. In chapter four, we can find our performance is not the best for low frequency selective environments, however, the methods with producing pseudo RR are outstanding in highly frequency selective scenarios. According to our simulation results, we also get good performances even the PDP is far beyond exponentially decay. For high mobility scenario, we can note that the methods combine with using of BEM with
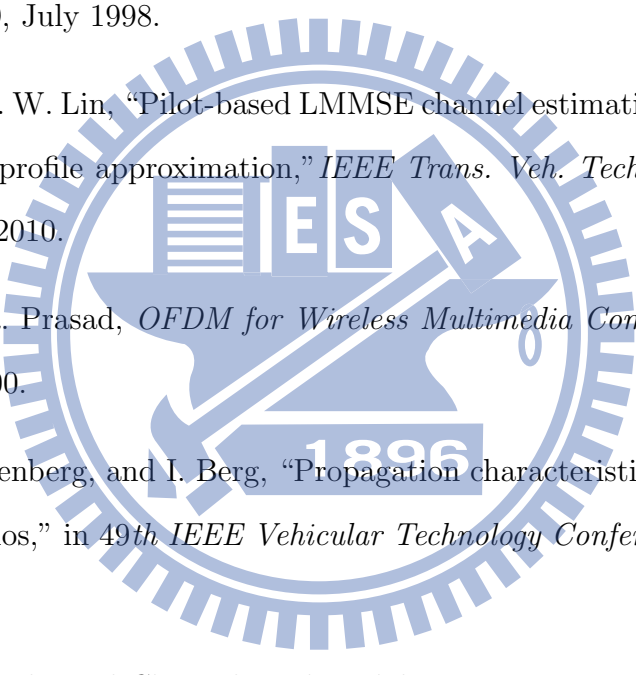
DPSS is better than combine with using linear interpolation method. Due to the features we mentioned above, we can use our cell phone with stable transmission by using these several methods. No matter how bad the environments are.

5.2 Future Work

There are several possible extension for our research:

- Add MIMO to the system for LTE and LTE-A.

- Try another techniques to estimate channel delay parameters.

- Try to estimate the vehicular speed for time variant channel estimation.

- Find an appropriate window length to balance DPSS performance and memories concerned.

- In this thesis, we do not consider the influence of intercarrier interference (ICI). The ICI simulation can be involved in the future.

- Change matlab code to C code and try to implement on DSP.

Bibliography

[1] O. Edfors, M. Sandell, J.-J. van de Beek, S. K. Wilson, and P. O. Borjesson, "OFDM channel estimation by singular value decomposition," *IEEE Trans. Commun.*, vol. 46, no. 7, pp. 931–939, July 1998.

[2] K.-C. Hung and D. W. Lin, "Pilot-based LMMSE channel estimation for OFDM systems with power-delay profile approximation," *IEEE Trans. Veh. Technology*, vol. 59, no. 1, pp 150–159, Jan. 2010.

[3] R. van Nee and R. Prasad, *OFDM for Wireless Multimedia Communications.* Boston: Artech House, 2000.

[4] J. Medbo, H. Hallenberg, and I. Berg, "Propagation characteristics at 5 GHz in typical radio-LAN scenarios," in *49th IEEE Vehicular Technology Conference*, vol. 1, 1999, pp. 185–189.

[5] 3GPP TS 36.211, *Physical Channels and Modulation.* V8.9.0, Dec. 2009.

[6] 3GPP TS 36.211, *Physical Channels and Modulation.* V10.7.0, Apr. 2013.

[7] Farooq Khan, *LTE for 4G Mobile Broadband: Air Interface Technologies and Performance.* Cambridge University Press, 2009.

[8] R. W. Chang, "Synthesis of band-limited orthogonal signals for multichannel data transmission," *Bell Systems Technical Journal*, vol. 45, pp. 1775–1798, Dec. 1966.

[9] B. Saltzberg, "Performance of an efficient parallel data transmission system," *IEEE Trans. Commun.*, vol. COM-15, no. 6, pp. 805–811, Dec. 1967.

[10] Y. S. Cho, J. Kim, W. Y. Yang, and C. G. Kang, *MIMO-OFDM Wireless Communications with MATLAB*. Wiley, 2010.

[11] M.-H. Hsieh, "Synchronization and channel estimation techniques for OFDM systems," Ph.D. dissertation, Department of Electronics Engineering and Institute of Electronics, National Chiao Tung Uni-versity, Hsinchu, Taiwan, R.O.C., May 1998.

[12] T. Zemen and C. F. Mecklenbrauker, "Time-variant channel estimation using discrete prolate spheroidal sequences," *IEEE Trans. Signal Process.*, vol. 53, no. 9, pp. 3597–3607, Sep. 2005.

[13] D. Slepian, "Prolate spheroidal wave functions, Fourier analysis, and uncertainty—V: the discrete case," *Bell Syst. Tech. Journal*, vol. 57, no. 5, pp. 1371–1430, May-Jun. 1978.

[14] Juo-Han Yu, "Research in LTE uplink channel estimation techniques," M.S. thesis, Department of Electronics Engineering and Institute of Electronics, National Chiao Tung University, Hsinchu, Taiwan, R.O.C., Oct. 2011.

作者簡歷

　　此篇論文作者為楊葆崧，新竹人，高中時期就讀於新竹科學園區實驗中學，大學及研究所就讀於交通大學電子工程系所，研究方向主要偏重於訊號處理、通訊演算法，然而大學及研究所也對於數位電路設計的範疇有所涉略。研究所指導教授為林大衛老師，碩士生涯為期兩年整。